# Electronic structure of turbostratic graphene

S. Shallcross,[1,*] S. Sharma,[2] E. Kandelaki,[1,3] and O. A. Pankratov[1]

[1]*Lehrstuhl für Theoretische Festkörperphysik, Staudstr. 7-B2, 91058 Erlangen, Germany*
[2]*Max-Planck Institute for Microstructure Physics, Weinberg 2, 06120 Halle, Germany*
[3]*Ruhr-Universität Bochum, Universitätsstrasse 150, 44801 Bochum, Germany*

We explore the rotational degree of freedom between graphene layers via the simple prototype of the graphene twist bilayer, i.e., two layers rotated by some angle $\theta$. It is shown that, due to the weak interaction between graphene layers, many features of this system can be understood by interference conditions between the quantum states of the two layers, mathematically expressed as Diophantine problems. Based on this general analysis we demonstrate that while the Dirac cones from each layer are always effectively degenerate, the Fermi velocity $v_F$ of the Dirac cones decreases as $\theta \rightarrow 0°$; the form we derive for $v_F(\theta)$ agrees with that found via a continuum approximation in [J. M. B. Lopes dos Santos, N. M. R. Peres, and A. H. Castro Neto, Phys. Rev. Lett. **99**, 256802 (2007)]. From tight-binding calculations for structures with $1.47° \leq \theta < 30°$ we find agreement with this formula for $\theta \gtrsim 5°$. In contrast, for $\theta \lesssim 5°$ this formula breaks down and the Dirac bands become strongly warped as the limit $\theta \rightarrow 0$ is approached. For an ideal system of twisted layers the limit as $\theta \rightarrow 0°$ is singular as for $\theta > 0$ the Dirac point is fourfold degenerate, while at $\theta = 0$ one has the twofold degeneracy of the *AB* stacked bilayer. Interestingly, in this limit the electronic properties are in an essential way determined *globally*, in contrast to the "nearsightedness" [W. Kohn, Phys. Rev. Lett. **76**, 3168 (1996)] of electronic structure generally found in condensed matter.

## I. INTRODUCTION

In addition to offering a possible route toward exploiting the many remarkable properties of graphene,[1] the epitaxial growth of graphene on SiC (Refs. [2–5]) presents a number of mysterious aspects. Principle amongst these is that the thermally induced growth of graphene on the C face typically results in several graphene layers and yet, remarkably, this complex graphene-based system shows behavior identical to that of single layer graphene (SLG). In striking contrast, bilayer graphene produced by mechanical exfoliation has already a different low energy electronic structure to that of SLG; a quadratic dispersion instead of linear.

An insight into this intriguing behavior of the C-face growth was recently provided by Hass *et al.*[6] These authors showed that growth on the C face results in a high density of twist boundary faults, i.e., layers with a relative rotation. Furthermore, *ab initio* calculations by the same authors showed that if two graphene layers were rotated with the same relative rotation observed in experiment, $\theta = 30° \pm 2.20°$, then these layers exhibited a linear spectrum near the Dirac point, exactly as in SLG. Rotation and translation of graphene layers thus have profoundly different impact on the low energy spectrum, and this lies at the heart of the C-face behavior.

While rationalizing the SLG nature of the C face, these findings raised a number of questions. Firstly, as to the character of the rotational degree of freedom in few layer graphene systems: do all rotations cause such an electronic decoupling or, alternatively, only a subset of "magic" angles? This question is relevant to experiments as subsequent investigations have shown that various angles of rotation may occur during growth on the C face.[5,7] Clearly, a related question is the nature of the mechanism responsible for this electronic decoupling: how does the rotation lead to the emergence of an effective Dirac-Weyl equation for low energies?

These questions, at first sight, appear difficult from the point of view of theory as one ultimately requires *general* statements to be made about an *infinite* class of possible lattices. Initially, theoretical progress was made by example of specific rotation angles or limits, with graphene bilayer and trilayer systems calculated *ab initio* in Ref. [8], while in Ref. [9] the $\theta \rightarrow 0°$ limit of the twist bilayer was investigated via a continuum approximation to the tight-binding Hamiltonian. In the former case a low energy linear spectrum was noted for all layers experiencing a relative rotation, while the latter work found also a linear spectrum but with the Fermi velocity at the Dirac point, $v_F$, strongly suppressed as compared to SLG. Subsequent Raman spectroscopy experiments[10,11] differ on whether this effect is present in misoriented graphene samples; in Ref. [10] a blueshift of the graphene two-dimensional (2D) peak was attributed to this effect, however in Ref. [11] this was instead attributed to a modification of the phonon dispersion in misoriented layers.

In Ref. [12] it was shown that the rotational degree of freedom was associated with a destructive interference of quantum states from each layer, and that this resulted in a coupling that becomes progressively weaker as the size of the commensuration cell increases. In fact, coupling at the Dirac point is already very weak for the smallest possible commensuration, a cell of 28 carbon atoms, with a splitting of 7 meV found in *ab initio* calculations.[12] All misoriented graphene layers are, therefore, predicted to show effectively decoupled Dirac cones.

Further theoretical investigations have been undertaken with regard to both the energetics of misoriented layers,[13] and the simulation of scanning tunneling microscopy images

for such layers.[14] In the former work it was noted that the sliding energy of relatively rotated graphene layers is essentially zero, in dramatic contrast to the case without rotation where the AB configuration is energetically favored. Most recently, tight-binding calculations have been performed for a wide range of misorientation angles.[15] This latter work demonstrates a reduction in the Fermi velocity that, for a wide range of rotation angles, agrees with the result of Ref. 9.

In this paper we aim to accomplish two things. Firstly, the formalism presented in Ref. 12 is extended to explain, on general lattice grounds (i.e., without deploying a continuum approximation), both the Dirac cone decoupling and Fermi velocity suppression. Secondly, we provide a numerical implementation of this formalism using the tight-binding method. We demonstrate that this numerical scheme is at least an order of magnitude faster than the usual tight-binding basis, and using this explore the electronic structure as a function of rotation angle for $1.47° \leq \theta < 30°$.

We now present a brief summary of the content of this paper. Firstly, in Sec. II we discuss in detail the crystal structure of mutually rotated graphene layers, and derive the conditions for a commensurate crystal structure to occur. An important feature of this system is the emergence, for $\theta \lesssim 15°$, of a so-called moiré pattern.[16] This is a hexagonal interference pattern, consisting of regions of AA and AB stacking, the periodicity of which represents a new structural length scale of the system.

Section III then describes the electronic structure of the bilayer in terms of a basis formed from the quantum states of the two mutually rotated layers with, in addition, the bilayer one-electron potential treated as a superposition of two single layer potentials, i.e. $V^{(1)} + \mathbf{R}V^{(2)}$ with $\mathbf{R}$ the rotation operator and $V^{(1,2)}$ potentials with the in-plane translation symmetry of SLG, an approach first described in Ref. 12. It is shown how this leads to a convenient separating out of purely symmetry related aspects of the electronic structure, leading to simple conditions for determining if the overlap elements of the potential with single layer states are vanishing or not. As the interlayer interaction part of the full bilayer Hamiltonian may be constructed from such overlap elements, an understanding of how and why these vanish leads in turn to an understanding of the nature of the interlayer decoupling in this system.

In this context we investigate how the overlap between states from the constituent layers depends on their **k** vectors (i.e., their **k** vectors in the two mutually rotated single layer Brillouin zones). We find that this dependence is rather subtle, and that the vanishing or not of such overlaps depends crucially on these **k** vectors. On this basis we demonstrate a number of general features of the bilayer electronic structure, and in particular show that (i) for the Dirac bands the first-order term of a perturbation theory in the interlayer interaction is negligible for all rotations and that, furthermore, (ii) second-order terms in perturbation theory lead to a Fermi velocity suppression of the form found in Ref. 9. We further develop two consequences of (i); if second (and higher) order terms are unimportant then the Dirac cones effectively decouple, and that the Dirac bands from each layer are degenerate regardless of the role of higher order terms.

Discussed also in this section is the rather unusual $\theta \to 0$ limit, which is a singular limit as for any $\theta > 0$ the electronic structure is dramatically different from that at $\theta = 0$. This is, of course, simply an electronic manifestation of the fact that the lattice geometry is also singular in this limit: for any small but nonzero $\theta$ one has a moiré pattern, while at $\theta = 0$ the graphene layers are simply AB (or AA3) stacked. An interesting aspect of this limit is a breakdown in the notion of "nearsightedness," i.e., that electronic properties are essentially determined locally. As the moiré periodicity diverges as $\theta \to 0°$ and, furthermore, as the twist bilayer electronic structure must, for any finite $\theta$, be different from both the AA and AB stacked bilayers, one concludes that in this limit the electronic properties are, in contrast, in an essential way determined globally.

Finally, Sec. IV is devoted to a presentation of tight-binding calculations for the graphene twist bilayer. We demonstrate that a basis formed by the quantum states of the two mutually rotated layers converges remarkably quickly, and leads to a dramatic improvement in computational efficiency. Using this we then investigate the bilayer electronic structure for $1.47° \leq \theta < 30°$ and find a suppression of the Fermi velocity, $v_F$, that is dramatic for small angles (at $\theta = 1.47°$ the reduction in $v_F$ is 95%) but, in agreement with all *ab initio* calculations to date,[6,8,12] insignificant for $\theta > \approx 15°$. However, while the expression for the Fermi velocity suppression derived here and in Ref. 9, describes almost perfectly the tight-binding results for $5° \leq \theta < 30°$, it breaks down for $\theta \lesssim 5°$. This breakdown is a result of the fact that the Fermi velocity suppression is a second-order effect in layer interaction, and in the limit $\theta \to 0°$ the resulting near degeneracy of the Dirac cones entails the importance of terms beyond this order.

## II. COMMENSURATION CONDITIONS OF THE TWISTED BILAYER

A prerequisite to exploring the electronic structure of the twisted bilayer is an elucidation of the crystallography of such a system, i.e., determining the conditions under which two misoriented layers are in commensuration. This problem was studied in Ref. 12 where a complete solution was presented; here we provide a more detailed derivation of those results with, additionally, a somewhat simpler and more symmetrical choice of commensuration vectors.

Evidently, the *existence* of a commensuration depends only on the relative rotation of the lattice vectors of each layer, and not on the structure of the unit cells of each layer. Thus we need not, at this stage, concern ourselves with which axis the rotation is taken about and the initial configuration (AB or AA, and so on) of the graphene bilayer; these amount to different choices of initial basis vectors within each cell. The commensuration condition may be written as

$$\mathbf{r}_1 = \mathbf{R}\mathbf{r}_2, \tag{1}$$

where $\mathbf{r}_1, \mathbf{r}_2$ are hexagonal lattice vectors, and $\mathbf{R}$ the rotation operator. The set $\{\mathbf{r}_1\}$ is the resulting coincident points between the two layers, while $\{\mathbf{r}_2\}$ is the same set, but viewed from the rotated coordinate system. Utilizing the unrotated

lattice as a coordinate system, i.e., $\mathbf{r}=i\mathbf{a}_1+j\mathbf{a}_2$ with $i,j \in \mathbb{Z}$, Eq. (1), with a standard choice of lattice vectors $\mathbf{a}_1=[\sqrt{3},0]$ and $\mathbf{a}_2=[\frac{\sqrt{3}}{2},3/2]$, may be written as

$$\begin{pmatrix} m_1 \\ m_2 \end{pmatrix} = \begin{pmatrix} \cos\theta - \dfrac{1}{\sqrt{3}}\sin\theta & -\dfrac{2}{\sqrt{3}}\sin\theta \\ \dfrac{2}{\sqrt{3}}\sin\theta & \cos\theta + \dfrac{1}{\sqrt{3}}\sin\theta \end{pmatrix} \begin{pmatrix} n_1 \\ n_2 \end{pmatrix}. \tag{2}$$

(Here and throughout this article our unit of length is chosen to be the graphene C-C separation.) This maps one integer pair $(n_1,n_2)$ to another $(m_1,m_2)$ and, for this to be possible, a necessary and sufficient condition on the matrix in Eq. (2) is that it assumes only rational values.[17] This leads to the following conditions on $\theta$:

$$\frac{1}{\sqrt{3}}\sin\theta = \frac{i_1}{i_3}, \tag{3}$$

$$\cos\theta = \frac{i_2}{i_3}, \tag{4}$$

where $i_1,i_2,i_3 \in \mathbb{N}$. These are therefore related by the following second order Diophantine equation

$$3i_1^2 + i_2^2 = i_3^2. \tag{5}$$

Solution of this equation proceeds in a standard way[18] (analogous to the case of Pythagorean triples) by dividing by $i_3^2$ and making the substitution $x=\frac{i_1}{i_3}$, $y=\frac{i_2}{i_3}$. There is thus a one to one mapping between solutions of Eq. (5) and rational points on the ellipse $3x^2+y^2=1$. One such point is (0,1) and any other may be found by the intersection with the ellipse of a line passing through (0,1) and $(q/p,0)$. The coordinates of this latter point then lead to the following solution for $i_1,i_2,i_3$

$$i_1 = 2pq, \tag{6}$$

$$i_2 = 3q^2 - p^2, \tag{7}$$

$$i_3 = 3q^2 + p^2, \tag{8}$$

where $p,q \in \mathbb{N}$. From these equations we immediately find the set of rotation angles leading to commensurations,

$$\theta = \cos^{-1}\left(\frac{3q^2-p^2}{3q^2+p^2}\right). \tag{9}$$

For $q \geq p > 0$ this formula produces rotation angles that lie in the range $0 \leq \theta \leq 60°$. All other rotation angles are equivalent due to the symmetry of the hexagonal lattice. Clearly, the limit $p/q \rightarrow 0$ corresponds to $\theta \rightarrow 0°$ while, on the other hand, the limit $p/q \rightarrow 1$ corresponds to $\theta \rightarrow 60°$. Note that changing the sign of $p$ or $q$ sends $\theta \rightarrow -\theta$. Since the limit $\theta \rightarrow 60°$ is equivalent to $\theta \rightarrow 0°$ taken from below, and since formally little changes by the substitution $p \rightarrow -p$ or $q \rightarrow -q$, our focus in this work will be on angles in the range $0° \leq \theta \leq 30°$.

We also require the corresponding primitive vectors of the commensuration lattice. Substitution of Eqs. (3) and (4) into

TABLE I. Possible values that the parameter $\gamma$ can take.

| | $\delta=1$ | $\delta=3$ |
|---|---|---|
| $p$, $q$ odd | 6 | 2 |
| Otherwise | 3 | 1 |

Eq. (2) results in the following coupled linear Diophantine equations:

$$\begin{pmatrix} m_1 \\ m_2 \end{pmatrix} = \frac{1}{i_3} \begin{pmatrix} i_2 - i_1 & -2i_1 \\ 2i_1 & i_2 + i_1 \end{pmatrix} \begin{pmatrix} n_1 \\ n_2 \end{pmatrix}. \tag{10}$$

The solution of these equations follows by a similarity transform such that the matrix multiplying $(n_1 n_2)^T$ is diagonal. Crucially, the eigenvectors of this matrix are *independent* of $p,q$ and thus the problem is recast as coupled linear Diophantine equations that are *linear* in $p,q$. These may then be solved by inspection yielding the result that

$$\begin{pmatrix} n_1 \\ n_2 \end{pmatrix} = \alpha \begin{pmatrix} p+3q \\ -2p \end{pmatrix} + \beta \begin{pmatrix} 2p \\ -p+3q \end{pmatrix}, \tag{11}$$

$$\begin{pmatrix} m_1 \\ m_2 \end{pmatrix} = \alpha \begin{pmatrix} -p+3q \\ 2p \end{pmatrix} + \beta \begin{pmatrix} -2p \\ p+3q \end{pmatrix}, \tag{12}$$

with $\alpha,\beta$ are arbitrary constants such that $\mathbf{n}$ and $\mathbf{m}$ are integer valued. The final step is to determine the primitive vectors of the commensuration lattice. This calculation we present in Appendix A, and here quote only the result. The form of the commensuration vectors turns out to depend on a parameter $\delta = 3/\gcd(p,3)$. For the case where $\delta=1$ we find

$$\mathbf{t}_1 = \frac{1}{\gamma}\begin{pmatrix} p+3q \\ -2p \end{pmatrix}, \quad \mathbf{t}_2 = \frac{1}{\gamma}\begin{pmatrix} 2p \\ -p+3q \end{pmatrix}, \tag{13}$$

while for the case $\delta=3$ we find

$$\mathbf{t}_1 = \frac{1}{\gamma}\begin{pmatrix} -p-q \\ 2q \end{pmatrix}, \quad \mathbf{t}_2 = \frac{1}{\gamma}\begin{pmatrix} 2q \\ -p+q \end{pmatrix}, \tag{14}$$

where $\gamma = \gcd(3q+p,3q-p)$. Values that this parameter may take when $\gcd(p,q)=1$ are indicated in Table I.

Thus every possible commensuration between misoriented layers is *uniquely specified* by an integer pair $p \geq q > 0$ such that $\gcd(p,q)=1$. Given this we can completely characterize the commensuration; the rotation angle may be obtained from Eq. (9), while the lattice vectors are given by either Eqs. (13) or (14), depending on whether the parameter $\delta = 3/\gcd(p,3)$ assumes the values of 1 or 3, respectively. The various notations introduced in this derivation are illustrated in Fig. 1.

It is worth reflecting on the reason that two integers, $p$ and $q$, are needed to specify a commensuration while, on the other hand it is clear that any bilayer lattice (commensurate or incommensurate) is uniquely specified by a single number $\theta$. This is a consequence of the relation between the real and rational number fields: given a $\theta$ there are infinitely many choices of $p$ and $q$ in Eq. (9) such that $\theta$ may be reproduced to an arbitrary accuracy $\epsilon$.
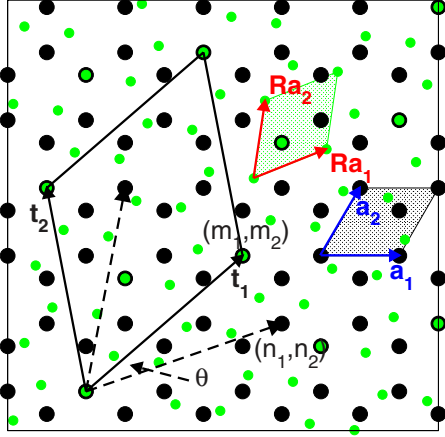
FIG. 1. (Color online) Illustration of the commensuration cell for the case of a misorientation angle of $\theta = 21.78°$, generated by a $(p,q)$ pair of (1,3) (lattice vectors $\mathbf{t}_1$ and $\mathbf{t}_2$). Shown also are the unit cells of the unrotated graphene layer (vectors $\mathbf{a}_1$, $\mathbf{a}_2$) and rotated graphene layer (vectors $\mathbf{Ra}_1$, $\mathbf{Ra}_2$). For explanations of other symbols refer to Sec. II.

The ratio of the total number of lattice vectors to coincident lattice vectors for the twist boundary is found to be given by

$$N = \frac{|(\mathbf{t}_1 \times \mathbf{t}_2) \cdot \hat{\mathbf{z}}|}{|(\mathbf{a}_1 \times \mathbf{a}_2) \cdot \hat{\mathbf{z}}|} = \frac{3}{\delta} \frac{1}{\gamma^2}(3q^2 + p^2), \qquad (15)$$

with the number of carbon atoms in the commensuration cell $N_C = 4N$. (The factor 4 simply arising from the fact there are two layers in the cell, and two basis atoms in the honeycomb structure.) In Fig. 2 is plotted $N_C$, as a function of misorientation angle; the minimum $N_C$ is 28 corresponding to $\theta$
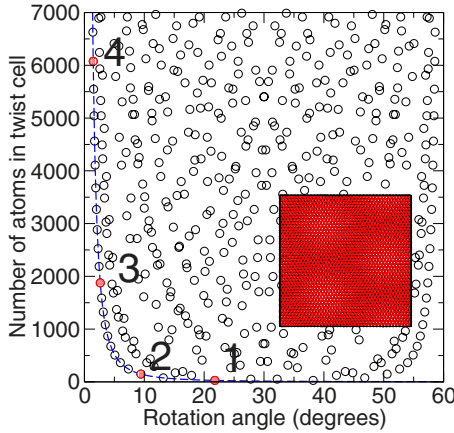


FIG. 2. (Color online) Shown is the number of C atoms, $N_C$, in the commensuration cell as a function of the relative orientation of the two graphene layers, for $N_C < 7000$. Inset displays the moiré pattern for the cell indicated number 4. Band structures of twist bilayers corresponding to the points labeled 1–4 are displayed in panels 1–4 of Fig. 8. The dashed line corresponds the lower bound $N_C = (\sin^2 \theta/2)^{-1}$; for commensuration cells that fall on this line the moiré periodicity is equal to the commensuration periodicity, see Sec. II for details.

$= 30° \pm 8.21$, however $N_C$ diverges in the $\theta \to 0°$ (or $\theta \to 60°$) limits. Combining Eqs. (9) and (15) we find that

$$N = \frac{3}{\gamma^2 \delta} \frac{p^2}{\sin^2 \theta/2}. \qquad (16)$$

and so for $\theta \to 0°$ $N$ diverges as $1/\theta^2$. This small angle limit is associated with the emergence of a new structural length scale, that of the moiré periodicity $D$; such a moiré pattern is shown in the inset of Fig. 2. The relation between $D$ and $\theta$ is given by[19]

$$D = \frac{a}{2 \sin \theta/2}. \qquad (17)$$

where $a$ is the graphene lattice constant. The relation between the lattice constant of the commensuration cell and the moiré periodicity may be seen by setting $p = 1$, $\delta = 3$, $\gamma = 2$ in Eq. (16), (corresponding to cells generated by $p = 1$ and $q$ an odd integer, see Table I), and using $N = D^2/a^2$ which then gives back the formula for the moiré periodicity, Eq. (17). In this case, therefore, the moiré periodicity is equal to the commensuration cell lattice constant. For these commensuration cells we find $N_C = (\sin^2 \theta/2)^{-1}$, and this is the lower bound function plotted in Fig. 2. On the other hand, for all other commensuration cells the "commensuration periodicity" is greater than the moiré periodicity.

Finally, we note that the analytic results presented here are in agreement with the numerical solution to this problem provided recently by Campenara *et al.*;[16] special cases of these results have been found in Ref. 9 (the case $p = 1$, $\delta = 3$, $\gamma = 2$) and more recently in Ref. 15 (the case $\delta = 1$).

## III. ANALYSIS OF THE INTERLAYER INTERACTION

In this section we shall describe how the problem of understanding the *general* electronic properties of the twist bilayer *for any* $\theta$ is solved. Our approach is that described in Ref. 12 which, in broad outline, may be characterized as "constructing the bilayer system from single layer components." We take the bilayer potential as a superposition of single layer potentials, and use as a basis for this new system the eigenkets of the single layer systems. The advantage of this is that the resulting matrix elements may then be analyzed as a commensuration problem of reciprocal space lattices. Such commensuration problems can be readily understood for any angle, and thus one may then understand the physics of the twist bilayer for general angle.

The remainder of this section proceeds as follows. In Sec. III A we first setup the Hamiltonian and basis used to analyze the twist bilayer. Following this, in Sec. III B the various reciprocal lattices and associated Brillouin zones are described. In Sec. III C a condition is derived that determines the vanishing of overlap elements found in the model of Sec. III A. Finally, in Secs. III D–III F, we use this understanding to determine a number of generic electronic properties of the twist bilayer.

### A. Model Hamiltonian and basis

In considering the interaction between misoriented layers it is useful to take the bilayer potential as simply the superposition of two single layer potentials, i.e.,

$$\mathbf{H} = \frac{\mathbf{p}^2}{2m} + \mathbf{V}^{(1)} + \mathbf{V}^{(2)}. \tag{18}$$

Here $\mathbf{V}^{(n)}$ are one-electron single layer graphene potential operators that satisfy

$$\mathbf{H}^{(n)}|\phi_{i\mathbf{k}}^{(n)}\rangle = \left(\frac{\mathbf{p}^2}{2m} + \mathbf{V}^{(n)}\right)|\phi_{i\mathbf{k}}^{(n)}\rangle = \epsilon_{i\mathbf{k}}^{(n)}|\phi_{i\mathbf{k}}^{(n)}\rangle, \tag{19}$$

where $\epsilon_{i\mathbf{k}}^{(n)}$ are SLG eigenvalues, and $i$ and $\mathbf{k}$ represent band and $\mathbf{k}$-vector quantum numbers, respectively. These one-electron SLG potentials are invariant under different in-plane translations; we have $\mathbf{T}\mathbf{V}^{(1)} = \mathbf{V}^{(1)}$ and $\mathbf{R}\mathbf{T}\mathbf{R}^{-1}\mathbf{V}^{(2)} = \mathbf{V}^{(2)}$. We shall take the superscript "1" to denote objects associated with the unrotated layer, and superscript "2" for objects associated with the rotated layer. (Such a designation is, in *mutually* rotated layers, clearly arbitrary and made only for convenience.) Given the weak interaction (and thus large separation) of the graphene layers, this approximation of the bilayer potential as a superposition of single layer potentials is expected to be good, but, in any case, is certainly sufficient for the qualitative understanding presented here.

As a basis for this Hamiltonian we take the combined eigenkets of the unrotated and rotated layers, i.e. $\{|\phi_{i_1\mathbf{k}_1}^{(1)}\rangle\}, \{|\phi_{i_2\mathbf{k}_2}^{(2)}\rangle\}$. One should note that since each SLG basis set by itself is complete on $\mathbb{R}^3$, this is generally an overcomplete basis set. On the other hand for minimal basis methods, such as the $p_z$ tight-binding method in which the basis consists of a $p_z$ atomic orbital centered at every site in the crystal, a bilayer basis set consisting of the combined eigenkets from each layer is clearly isomorphic to the usual basis set that would be employed.

### B. Reciprocal space properties of the bilayer system

Here we describe the reciprocal space lattices corresponding to the various real space lattices introduced in Sec. II. First a note of nomenclature; we denote the reciprocal lattice vectors corresponding to the unrotated (rotated) real space vectors $\mathbf{a}_1$ and $\mathbf{a}_2$ ($\mathbf{R}\mathbf{a}_1$ and $\mathbf{R}\mathbf{a}_2$) by $\mathbf{b}_1$ and $\mathbf{b}_2$ ($\mathbf{R}\mathbf{b}_1$ and $\mathbf{R}\mathbf{b}_2$), while the reciprocal space lattice vectors corresponding to the real space commensuration vectors $\mathbf{t}_1$ and $\mathbf{t}_2$ are denoted by $\mathbf{g}_1$ and $\mathbf{g}_2$. We shall refer to this latter reciprocal space lattice as the bilayer reciprocal lattice.

The vectors $\mathbf{g}_1$ and $\mathbf{g}_2$ are found from Eq. (13) to be

$$\mathbf{g}_1 = \frac{\gamma}{3(3q^2 + p^2)}[(p + 3q)\mathbf{b}_1 + 2p\mathbf{b}_2], \tag{20}$$

$$\mathbf{g}_2 = \frac{\gamma}{3(3q^2 + p^2)}[-2p\mathbf{b}_1 - (p - 3q)\mathbf{b}_2], \tag{21}$$

for the case where $\delta = 1$ and from Eq. (14), to be

$$\mathbf{g}_1 = \frac{\gamma}{3q^2 + p^2}[-(p - q)\mathbf{b}_1 + 2q\mathbf{b}_2], \tag{22}$$
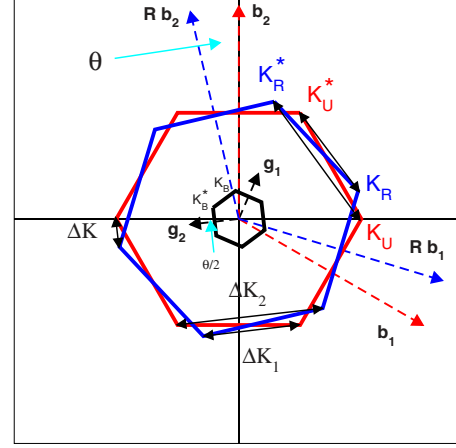


FIG. 3. (Color online) Brillouin zones of the unrotated (U) and rotated (R) graphene layers, as well as the Brillouin zone of the bilayer supercell (B) for the case $(p,q) = (1,5)$, corresponding to $\theta = 13.17°$. In this Figure $\mathbf{b}_1$, $\mathbf{b}_2$ are the reciprocal lattice vectors of the unrotated graphene layer, $\mathbf{R}\mathbf{b}_1$, $\mathbf{R}\mathbf{b}_2$ the reciprocal lattice vectors of the rotated layer, and $\mathbf{g}_1$, $\mathbf{g}_2$ the reciprocal lattice vectors of the bilayer supercell. Special $K$ points of various Brillouin zones indicated by subscript U, R, and B. The separations of special $K$ points indicated are $\Delta K = |\mathbf{K}_R - \mathbf{K}_U| = |\mathbf{K}_R^* - \mathbf{K}_U^*|$, $\Delta K_1 = |\mathbf{K}_U^* - \mathbf{K}_R|$, and $\Delta K_2 = |\mathbf{K}_U - \mathbf{K}_R^*|$.

$$\mathbf{g}_2 = \frac{\gamma}{3q^2 + p^2}[-2q\mathbf{b}_1 - (p + q)\mathbf{b}_2], \tag{23}$$

for the case $\delta = 3$. The Brillouin zones associated with each of these sets of primitive vectors, $\{\mathbf{b}_1, \mathbf{b}_2\}$, $\{\mathbf{R}\mathbf{b}_1, \mathbf{R}\mathbf{b}_2\}$, and $\{\mathbf{g}_1, \mathbf{g}_2\}$, are shown in Fig. 3 for the twist bilayer $(p,q) = (1,5)$. For convenience of exposition these Brillouin zones (BZ) will be referred to by the abbreviations UBZ (for the unrotated BZ), RBZ (for the rotated BZ), and BBZ for the BZ of the bilayer reciprocal lattice.

These bilayer reciprocal lattice vectors determine a map by which $\mathbf{k}$ vectors in the UBZ and RBZ are related to those of the BBZ (the usual so-called "folding back" condition of $\mathbf{k}$ vectors). It should be emphasized at this point that there are three separate $\mathbf{k}$ indices in the problem as it is formulated here. We have a $\mathbf{k}$ vector in the BBZ which is a good quantum number for the bilayer Hamiltonian and eigenkets, but we also have the $\mathbf{k}$ indices of the single layer basis used to solve the Hamiltonian at this $\mathbf{k}$, labeled by $\mathbf{k}_1$ and $\mathbf{k}_2$. To solve the Hamiltonian at $\mathbf{k}$, the single layer basis then consists of all those eigenkets which map back from the UBZ and RBZ to the point $\mathbf{k}$ in the BBZ.

An interesting, and for the nature of the interlayer interaction crucial, relationship exists between the special $K$ points of all these BZ's: to each special $K$ point of the BBZ is mapped back one of the special $K$ point from the UBZ and one from the RBZ. The precise manner in which this happens depends in a rather complex way on the $p$, $q$ parameters of the commensuration, detailed in Tables II and III. The overall scheme, however, is clear: for commensurations characterized by $\delta = 1$ $K$ points connected by $\Delta K$ (see Fig. 3) map to the same special $K$ point of the BBZ while, for $\delta = 3$, it is

TABLE II. Structure of the mapping of special $K$ points of the unrotated (U) and rotated (R) layer Brillouin zones to the special $K$ points of the bilayer (B) Brillouin zone, for the case $\delta=1$. The designation of the special $K$ points corresponds to that of Fig. 3.

|  | $\gamma=3$ | $\gamma=6$ |
|---|---|---|
| $\mathrm{mod}(q,3)=1$ | $\mathbf{K}_U \to \mathbf{K}_B$ | $\mathbf{K}_U \to \mathbf{K}_B^*$ |
|  | $\mathbf{K}_U^* \to \mathbf{K}_B^*$ | $\mathbf{K}_U^* \to \mathbf{K}_B$ |
|  | $\mathbf{K}_R \to \mathbf{K}_B$ | $\mathbf{K}_R \to \mathbf{K}_B^*$ |
|  | $\mathbf{K}_R^* \to \mathbf{K}_B^*$ | $\mathbf{K}_R^* \to \mathbf{K}_B$ |
| $\mathrm{mod}(q,3)=2$ | $\mathbf{K}_U \to \mathbf{K}_B^*$ | $\mathbf{K}_U \to \mathbf{K}_B$ |
|  | $\mathbf{K}_U^* \to \mathbf{K}_B$ | $\mathbf{K}_U^* \to \mathbf{K}_B^*$ |
|  | $\mathbf{K}_R \to \mathbf{K}_B^*$ | $\mathbf{K}_R \to \mathbf{K}_B$ |
|  | $\mathbf{K}_R^* \to \mathbf{K}_B$ | $\mathbf{K}_R^* \to \mathbf{K}_B^*$ |

the conjugate pairs $(K_U^*, K_R)$ and $(K_U, K_R^*)$, separated by $\Delta K_1$ and $\Delta K_2$, respectively, that map back to the same special $K$ points of the BBZ (these special $K$ points and their separations are indicated also in Fig. 3).

Thus without any layer interaction, i.e., what translational symmetry alone requires, is that the Dirac cones from the unrotated and rotated layers are mapped to the special $K$ points of the BBZ. With no layer interaction we therefore find two degenerate Dirac cones situated at each special $K$ point of the BBZ. It should be stressed that this mapping is particular to the $K$ star; a similar map does not, for example, exist for the $M$ star. Interestingly, this implies that $M$-point chiral fermions (which may be generated by the application of a periodic scalar potential[20]) would behave rather differently in this context.

We may now consider what happens to this degeneracy when we turn on a layer interaction. In general, of course, such an interaction would result in a splitting of the Dirac cones, however this is not what happens for the case of mutually rotated graphene layers. The key to understanding this, as we now describe, lies in the remarkable behavior of the overlap elements of the bilayer Hamiltonian, Eq. (18), with states from the mutually rotated graphene layers.

TABLE III. Structure of the mapping of special $K$ points of the unrotated (U) and rotated (R) layer Brillouin zones to the special $K$ points of the bilayer (B) Brillouin zone, for the case $\delta=3$. The designation of the special $K$ points corresponds to that of Fig. 3.

|  | $\gamma=1$ | $\gamma=2$ |
|---|---|---|
| $\mathrm{mod}(p,3)=1$ | $\mathbf{K}_U \to \mathbf{K}_B^*$ | $\mathbf{K}_U \to \mathbf{K}_B$ |
|  | $\mathbf{K}_U^* \to \mathbf{K}_B$ | $\mathbf{K}_U^* \to \mathbf{K}_B^*$ |
|  | $\mathbf{K}_R \to \mathbf{K}_B$ | $\mathbf{K}_R \to \mathbf{K}_B^*$ |
|  | $\mathbf{K}_R^* \to \mathbf{K}_B^*$ | $\mathbf{K}_R^* \to \mathbf{K}_B$ |
| $\mathrm{mod}(p,3)=2$ | $\mathbf{K}_U \to \mathbf{K}_B$ | $\mathbf{K}_U \to \mathbf{K}_B^*$ |
|  | $\mathbf{K}_U^* \to \mathbf{K}_B^*$ | $\mathbf{K}_U^* \to \mathbf{K}_B$ |
|  | $\mathbf{K}_R \to \mathbf{K}_B^*$ | $\mathbf{K}_R \to \mathbf{K}_B$ |
|  | $\mathbf{K}_R^* \to \mathbf{K}_B$ | $\mathbf{K}_R^* \to \mathbf{K}_B^*$ |

## C. Matrix elements of the bilayer Hamiltonian

Given a bilayer potential of the form $\mathbf{V}^{(1)}+\mathbf{V}^{(2)}$, and a basis set of single layer eigenkets $\{|\phi_{i_1\mathbf{k}_1}^{(1)}\rangle\}, \{|\phi_{i_2\mathbf{k}_2}^{(2)}\rangle\}$, the electronic structure will be determined by *interlayer* matrix elements of the type $\langle\phi_{i_1\mathbf{k}_1}^{(1)}|\mathbf{V}^{(1)}|\phi_{i_2\mathbf{k}_2}^{(2)}\rangle$. Using this matrix element as a specific example, we now show how one may derive a general condition that determines whether such a matrix element vanishes or not. Using a plane-wave expansion for each of the objects in this matrix element, i.e.,

$$\mathbf{V}^{(1)} = \sum_{\mathbf{G}_1'} V_{\mathbf{G}_1'}^{(1)} e^{i\mathbf{G}_1'\cdot\mathbf{r}}, \qquad (24)$$

$$\phi_{i_1\mathbf{k}_1}^{(1)*}(z) = \sum_{\mathbf{G}_1''} c_{i_1\mathbf{k}_1+\mathbf{G}_1''}^{(1)*}(z) e^{-i(\mathbf{k}_1+\mathbf{G}_1'')\cdot\mathbf{r}}, \qquad (25)$$

$$\phi_{i_2\mathbf{k}_2}^{(2)}(z) = \sum_{\mathbf{RG}_2} c_{i_2\mathbf{k}_2+\mathbf{RG}_2}^{(2)}(z) e^{i(\mathbf{k}_2+\mathbf{RG}_2)\cdot\mathbf{r}}, \qquad (26)$$

we find

$$\langle\phi_{i_1\mathbf{k}_1}^{(1)}|\mathbf{V}^{(1)}|\phi_{i_2\mathbf{k}_2}^{(2)}\rangle = \sum_{\mathbf{G}_1,\mathbf{RG}_2}\left(\sum_{\mathbf{G}_1'}\int dz\, c_{i_1\mathbf{k}_1+\mathbf{G}_1+\mathbf{G}_1'}^{(1)*}(z)\right.$$
$$\left. \times V_{\mathbf{G}_1'}^{(1)}(z) c_{i_2\mathbf{k}_2+\mathbf{RG}_2}^{(2)}(z)\right)\delta_{\mathbf{k}_1+\mathbf{G}_1=\mathbf{k}_2+\mathbf{RG}_2}$$
$$= \sum_{\mathbf{G}_1,\mathbf{RG}_2} C_{\mathbf{k}_1+\mathbf{G}_1}^{\mathbf{k}_2+\mathbf{RG}_2}\delta_{\mathbf{k}_1+\mathbf{G}_1=\mathbf{k}_2+\mathbf{RG}_2}, \qquad (27)$$

where we have made the convenient substitution $\mathbf{G}_1''-\mathbf{G}_1' =\mathbf{G}_1$. As the structure of Eq. (27) arises simply from the differing in-plane translation groups of the constituent objects, any such interlayer matrix element may be cast into this form (although the coefficients $C_{\mathbf{k}_1+\mathbf{G}_1}^{\mathbf{k}_2+\mathbf{RG}_2}$ will obviously be different).

Clearly, it is the Kronecker delta term in Eq. (27) that is the most significant consequence of rotation. This Kronecker delta term ensures that in the double sum over $\mathbf{G}_1$ and $\mathbf{RG}_2$ only terms satisfying

$$\mathbf{G}_1 = \mathbf{RG}_2 + \mathbf{k}_2 - \mathbf{k}_1 \qquad (28)$$

contribute. This is just a commensuration condition between the reciprocal lattices of the unrotated and rotated layers. However, in contrast to the real space commensuration condition, $\mathbf{a}_1=\mathbf{Ra}_2$, this involves not only the geometry via the $\mathbf{R}$ operator, but also a dependence on the single layer states through the term $\mathbf{k}_2-\mathbf{k}_1$. This removal of contributions from the interlayer matrix elements is a direct consequence of the mutual rotation of the layers, and can be seen as a destructive interference of the quantum states from each layer. It is now clear that the advantage of the approach deployed here is that we have separated the symmetry aspects of the problem, which generate a *selection condition* for the coefficients $C_{\mathbf{k}_1+\mathbf{G}_1}^{\mathbf{k}_2+\mathbf{RG}_2}$, from details of the electronic structure which are contained in the actual values of these coefficients.

Continuity of wave functions and potentials in real space implies that these coefficients will decay to zero with increasing $|\mathbf{G}_{1,2}|$ and will be largest for $\mathbf{G}_{1,2}$ at or near the
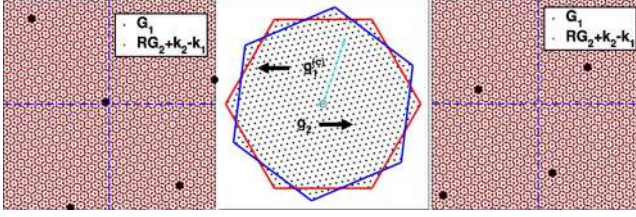
FIG. 4. (Color online) Example of the relationship between $\mathbf{k}_2 - \mathbf{k}_1$ and the shift of the lattice of solution vectors of the equation $\mathbf{G}_1 = \mathbf{R}\mathbf{G}_2 + \mathbf{k}_2 - \mathbf{k}_1$. Shown in the middle panel are those $\mathbf{k}$ points that fold back to the $\Gamma$ point of the commensuration Brillouin zone, for the case $(p, q) = (11, 31)$. The left and right panels display the reciprocal lattices $\mathbf{G}_1$ and $\mathbf{R}\mathbf{G}_2 + \mathbf{k}_2 - \mathbf{k}_1$ along with the solution vectors for the two different cases of $\mathbf{k}_2 - \mathbf{k}_1$ indicated in the central panel. See Sec. III E for details.

origin. In addition, the coincident points between the lattices $\mathbf{G}_1$ and $\mathbf{R}\mathbf{G}_2 + \mathbf{k}_2 - \mathbf{k}_1$ become increasingly separated as $\theta \rightarrow 0°$ (just as the size of the real space commensuration cell diverges in this limit, see Sec. II). Since these coincident points represent the only symmetry allowed contributions to the bilayer matrix elements, we see that for sufficiently small $\theta$ there can be *at most one contributing term*, which occurs in the case of a coincident point close to the origin of reciprocal space. For example, if $\mathbf{k}_1 = \mathbf{k}_2$ in Eq. (28) then $\mathbf{G}_1 = \mathbf{R}\mathbf{G}_2 = 0$ is a solution and, as the coefficient $C_0^0$ is generally nonzero, so in turn will the matrix element will remain finite for all $\theta$. On the other hand, in the case where all coincident points are sufficiently far from the origin, the matrix element will vanish for sufficiently small $\theta$. (An illustration of these two cases is given in the left and right hand side panels of Fig. 4).

As we shall now show the term $\mathbf{k}_2 - \mathbf{k}_1$ in Eq. (28) results simply in a shift from the origin of the commensuration lattice (i.e., the lattice of coincident points) that would be found for the case $\mathbf{k}_2 - \mathbf{k}_1 = 0$. The relation between the term $\mathbf{k}_2 - \mathbf{k}_1$ and this shift, which can be found by solving Eq. (28), thus plays a crucial role in determining which bilayer matrix elements will vanish.

The solution follows by the casting of Eq. (28) into a Diophantine problem, exactly as outlined in Sec. II for the real space case. This, and the solution of the resulting Diophantine problem, are described in Appendix B. Here we summarize the results with the solutions expressed in terms of the unrotated reciprocal lattice vectors as $m_1 \mathbf{b}_1 + m_2 \mathbf{b}_2$. One finds that for the case $\delta = 1$ two possible solutions given by

$$\mathbf{m} = \alpha \frac{1}{\gamma}\begin{pmatrix} p + 3q \\ 2p \end{pmatrix} + \beta \frac{1}{\gamma}\begin{pmatrix} -2p \\ -p + 3q \end{pmatrix} + \frac{\gamma}{6q}\begin{pmatrix} l_1 \\ l_2 \end{pmatrix} \quad (29)$$

and

$$\mathbf{m} = \alpha \frac{1}{\gamma}\begin{pmatrix} p + 3q \\ 2p \end{pmatrix} + \beta \frac{1}{\gamma}\begin{pmatrix} -2p \\ -p + 3q \end{pmatrix} + \frac{\gamma}{6p}\begin{pmatrix} l_1 - 2l_2 \\ 2l_1 - l_2 \end{pmatrix}. \quad (30)$$

While for the case $\delta = 3$ one finds

$$\mathbf{m} = \alpha \frac{1}{\gamma}\begin{pmatrix} -p + q \\ 2q \end{pmatrix} + \beta \frac{1}{\gamma}\begin{pmatrix} 2q \\ p + q \end{pmatrix} - \frac{\gamma}{2p}\begin{pmatrix} l_1 \\ l_2 \end{pmatrix} \quad (31)$$

and

$$\mathbf{m} = \alpha \frac{1}{\gamma}\begin{pmatrix} -p + q \\ 2q \end{pmatrix} + \beta \frac{1}{\gamma}\begin{pmatrix} 2q \\ p + q \end{pmatrix} + \frac{\gamma}{6q}\begin{pmatrix} l_1 - 2l_2 \\ 2l_1 - l_2 \end{pmatrix}. \quad (32)$$

Here $\alpha$ and $\beta$ are arbitrary integers, $\gamma = \gcd(3q + q, 3q - p)$, and $l_1$ and $l_2$ are the integers that result when $\mathbf{k}_2 - \mathbf{k}_1$ is expressed in coordinates of the bilayer reciprocal lattice, i.e.,

$$\mathbf{k}_2 - \mathbf{k}_1 = l_1 \mathbf{g}_1 + l_2 \mathbf{g}_2. \quad (33)$$

(Note that since both $\mathbf{k}_1$ and $\mathbf{k}_2$ fold back, under translations by the bilayer reciprocal lattice vectors $\mathbf{g}_1$ and $\mathbf{g}_2$, to the same $\mathbf{k}$ point of the BBZ then their difference can be expressed as integer multiples of $\mathbf{g}_1$ and $\mathbf{g}_2$. Hence in coordinates of the bilayer reciprocal lattice the difference $\mathbf{k}_2 - \mathbf{k}_1$ will always be integer.) Clearly, in all cases the solutions are of the form

$$\alpha \widetilde{\mathbf{G}}_1 + \beta \widetilde{\mathbf{G}}_2 + \Delta \widetilde{\mathbf{G}}, \quad (34)$$

with the important constant shift $\Delta \widetilde{\mathbf{G}}$ determined by $\mathbf{k}_2 - \mathbf{k}_1$.

It should be noted that these expressions provide only a partial solution to Eq. (28). The reason is for this is that while $(m_1, m_2)$ must be integer valued, the shift terms are obviously not integer valued unless, e.g., both $l_1$ and $l_2$ are divisible by $6q/\gamma$ in Eq. (29). This absence of a complete solution is due to the fact that, as shown in Appendix B, Eq. (28) results in an *inhomogeneous* simultaneous linear Diophantine problem (in contrast to the homogeneous problem of the real space commensuration) which is known to have no analytic solution. However, as we now demonstrate, this partial solution provides sufficient insight into the selection rule, Eq. (28), that several generic features of the bilayer electronic structure may be elucidated.

### D. Decoupling of the Dirac cones

Here we shall prove that for all commensuration cells with $N_C$ greater than some critical value the Dirac bands from the unrotated and rotated layers will be effectively degenerate in energy. Thus there will be a fourfold degeneracy at the Dirac points of the bilayer band structure, with the Dirac bands themselves twofold degenerate. While this derivation demonstrates the *existence* of such a critical value, the numerical value of this parameter will depend on the coefficients $C_{\mathbf{k}_1 + \mathbf{G}_1}^{\mathbf{k}_2 + \mathbf{R}\mathbf{G}_2}$ and can, of course, only be determined by actual calculation of the electronic structure.

It should be stressed that this result requires only (i) mutually rotated and weakly interacting layers of hexagonal symmetry and (ii) the low energy spectrum to located at the vectors of the $K$ star; it is, therefore, applicable to other contexts in which graphene may be created.

Our approach is based on a perturbative treatment and the use of the selection rules for terms in the matrix element sums derived in the previous section. Since in the absence of any interlayer interaction we have two degenerate Dirac cones at the special $K$ points of the BBZ (see Sec. III B), then the first-order energy shift will be given by the secular

equation of degenerate state perturbation theory.

One should note that, without interaction, the degeneracy at and away from the Dirac points will be different: fourfold at the Dirac point and twofold away. In fact, as our considerations are entirely based on the in-plane translation groups, and not on point group symmetry arguments, then there will be no fundamental difference in how we treat these two cases, and for simplicity we consider here the case of a two-fold degeneracy. The resulting secular equation is then

$$\begin{pmatrix} \delta H_{11} & \delta H_{12} \\ \delta H_{21} & \delta H_{22} \end{pmatrix} \begin{pmatrix} a_1 \\ a_2 \end{pmatrix} = \delta \epsilon_i^{(1)} \begin{pmatrix} a_1 \\ a_2 \end{pmatrix}, \tag{35}$$

where the elements $\delta H_{ij}$ are given by

$$\delta H_{11} = \langle \phi_{i_1 \mathbf{k}_1}^{(1)} | \mathbf{V}^{(2)} | \phi_{i_1 \mathbf{k}_1}^{(1)} \rangle, \tag{36}$$

$$\delta H_{12} = \frac{1}{2} (\epsilon_{i_1 \mathbf{k}_1}^{(1)} + \epsilon_{i_2 \mathbf{k}_2}^{(2)}) \langle \phi_{i_1 \mathbf{k}_1}^{(1)} | \phi_{i_2 \mathbf{k}_2}^{(2)} \rangle + \langle \phi_{i_1 \mathbf{k}_1}^{(1)} | \overline{\mathbf{V}} | \phi_{i_2 \mathbf{k}_2}^{(2)} \rangle, \tag{37}$$

$$\delta H_{21} = \frac{1}{2} (\epsilon_{i_1 \mathbf{k}_1}^{(1)} + \epsilon_{i_2 \mathbf{k}_2}^{(2)}) \langle \phi_{i_2 \mathbf{k}_2}^{(2)} | \phi_{i_1 \mathbf{k}_1}^{(1)} \rangle + \langle \phi_{i_2 \mathbf{k}_2}^{(2)} | \overline{\mathbf{V}} | \phi_{i_1 \mathbf{k}_1}^{(1)} \rangle, \tag{38}$$

$$\delta H_{22} = \langle \phi_{i_2 \mathbf{k}_2}^{(2)} | \mathbf{V}^{(1)} | \phi_{i_2 \mathbf{k}_2}^{(2)} \rangle, \tag{39}$$

and with $\overline{\mathbf{V}} = (\mathbf{V}^{(1)} + \mathbf{V}^{(2)})/2$. Here $(i_1, \mathbf{k}_1)$ and $(i_2, \mathbf{k}_2)$ are the **k** vectors and band indices of the states from the Dirac cones of the UBZ and RBZ that map to the BBZ Dirac cone.

Using the approach of the previous section we can now determine when the matrix elements involved in Eqs. (36) and (37) vanish. In particular, we know that for a sufficiently small misorientation $\theta$ the vanishing or not of these matrix elements is governed solely by the shift term $\Delta \widetilde{\mathbf{G}}$, i.e. by $\mathbf{k}_2 - \mathbf{k}_1$.

To determine $\Delta \widetilde{\mathbf{G}}$ we must therefore specify the difference $\mathbf{k}_2 - \mathbf{k}_1$, that is the difference between the **k** vectors of the two single layer Dirac cone states that map back to the same **k** vector in the BBZ. If we consider the case $\delta = 3$ then, reading from Table III, we find that the special $K$-point pair $(\mathbf{K}_U^*, \mathbf{K}_R)$, or its conjugate pair, is folded back to the same special $K$ point in the BBZ. Clearly **k**-point differences are unchanged by shifting all **k** points by some $\delta \mathbf{k}$, and therefore $\mathbf{k}_2 - \mathbf{k}_1 = \mathbf{K}_U^* - \mathbf{K}_R$.

Expressing $\mathbf{K}_U^* - \mathbf{K}_R$ in coordinates of the bilayer reciprocal lattice we then find $\mathbf{K}_U^* - \mathbf{K}_R = (q - p)/(2\gamma)(\mathbf{g}_1 + \mathbf{g}_2)$, i.e., that $l_1 = l_2 = (q - p)/(2\gamma)$ in Eq. (33). Using this and substituting into the shift term of Eq. (31) we find

$$\Delta \widetilde{\mathbf{G}} = -\frac{q - p}{2p} \begin{pmatrix} 1 \\ 1 \end{pmatrix}. \tag{40}$$

We can easily ensure this is integer valued (as it must be) by the choice $q = p(1 + 2n)$, with $n$ an integer. We thus conclude that both the commensuration reciprocal lattice vectors *and the shift from the origin* diverge as $q \to \infty$, that is, as $\theta \to 0°$. The first-order shift will therefore be *negligible for all q* that result in commensuration cells greater than some criti-
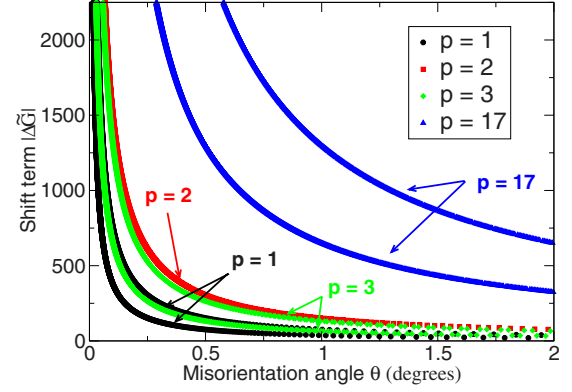


FIG. 5. (Color online) Shown is the shift term $|\Delta \widetilde{\mathbf{G}}|$ corresponding to the separations $\mathbf{k}_2 - \mathbf{k}_1 = \mathbf{K}_U^* - \mathbf{K}_R$ for $p = 1, 2, 17$ ($\delta = 3$), and $\mathbf{k}_2 - \mathbf{k}_1 = \mathbf{K}_U - \mathbf{K}_R$ for $p = 3(\delta = 1)$. Note that this shift diverges in all cases as $\theta \to 0$.

cal size, which will depend on the particular form of the $C_{\mathbf{k}_1 + \mathbf{G}_1}^{\mathbf{k}_2 + R\mathbf{G}_2}$, i.e., on details of the electronic structure.

If we reflect that as $\theta \to 0$ then both $\Delta K_1 = |\mathbf{K}_U^* - \mathbf{K}_R| \to 2/3$ and $\Delta K_2 = |\mathbf{K}_U - \mathbf{K}_R^*| \to 2/3$ while, at the same time, $g = |\mathbf{g}_1| = |\mathbf{g}_2| \to 0$ [see Eq. (42)], then it is not surprising that $\Delta \widetilde{\mathbf{G}}$ diverges. The behavior of $\Delta \widetilde{\mathbf{G}}$ in the case where $\delta = 1$ is, however, not so clear. In this case $K$ points separated by $\Delta K$ map back to the BBZ $K$ points, and so $\mathbf{k}_2 - \mathbf{k}_1 = \mathbf{K}_U - \mathbf{K}_R = \mathbf{K}_U^* - \mathbf{K}_R^*$, and this, as may be seen from Fig. 3 goes to zero as $\theta \to 0$. In this case neither Eqs. (29) or (30) yield an integer valued $\Delta \widetilde{\mathbf{G}}$ and so they may not be used. The Diophantine problem can, however, be solved numerically with the result that, as shown in Fig. 5, $|\Delta \widetilde{\mathbf{G}}|$ diverges as $\theta \to 0$ in this case also.

The question then arises if higher order terms in perturbation theory may lead to a *splitting* of the Dirac cones. In fact, it is easy to show that such terms may lead only to an *equal shift of both bands*. This can be seen by an examination of the quantities involved in higher orders of perturbation theory. Let us first consider the calculation of the shift of the unrotated layer Dirac band. All terms in the perturbation expansion (which we do not need to consider explicitly) will involve matrix elements $\langle \phi_{i_1 \mathbf{k}_1}^{(1)} | \overline{\mathbf{V}} | \phi_{i_2 \mathbf{k}_2}^{(2)} \rangle$ and $\langle \phi_{i_1 \mathbf{k}_1}^{(1)} | \mathbf{V}^{(2)} | \phi_{i_1 \mathbf{k}_1}^{(1)} \rangle$, and the unperturbed eigenvalues, which are just those of single layer graphene. Now, if we consider the shift of the rotated layer Dirac band we see that the relevant matrix elements are either the conjugate of those involved in the former case, $\langle \phi_{i_2 \mathbf{k}_2}^{(2)} | \overline{\mathbf{V}} | \phi_{i_1 \mathbf{k}_1}^{(1)} \rangle = \langle \phi_{i_1 \mathbf{k}_1}^{(1)} | \overline{\mathbf{V}} | \phi_{i_2 \mathbf{k}_2}^{(2)} \rangle^*$, or are equal by the symmetry of the bilayer, $\langle \phi_{i_2 \mathbf{k}_2}^{(2)} | \mathbf{V}^{(1)} | \phi_{i_2 \mathbf{k}_2}^{(2)} \rangle = \langle \phi_{i_1 \mathbf{k}_1}^{(1)} | \mathbf{V}^{(2)} | \phi_{i_1 \mathbf{k}_1}^{(1)} \rangle$. Since the unperturbed eigenvalue spectrum is again that of single layer graphene we immediately see that all terms in the perturbation expansion for the eigenvalue shift of the rotated and unrotated layers will be identical, and hence also the final energy shift.

Thus it is only the first-order term that can break the degeneracy of the Dirac cones from each layer and, as we have shown above, this is zero for all $N_C$ greater than some critical value. Since it is known from *ab initio* calculations[11] that this degeneracy is already very small for the smallest cell $N_C$

$=28$, corresponding to $(p,q)=(1,3)$, we can then conclude that *for all commensuration cells the Dirac bands will be effectively degenerate*, with exact degeneracy in the $\theta \to 0°$ limit or incommensurate rotations.

When higher order terms in the perturbation expansion are unimportant the enforced vanishing of the first-order term therefore leads to a decoupling of the Dirac cones. Higher orders in perturbation theory, while unable to split the Dirac cones, may, as we shall see subsequently, lead to a suppression of the Fermi velocity of the degenerate Dirac cones and nonlinear band warping for very small misorientation angles.

### E. Rotation angle versus cell geometry dependence of the coupling of single layer states

Given a relative rotation $\theta$ between the two graphene layers there exists an infinite set of integer pairs $(p,q)$ that, via Eq. (9), reproduce the rotation angle to arbitrary accuracy. This includes also incommensurate rotations, corresponding to the limit of diverging $p$ and $q$. Each of the bilayer unit cells in this set have differing in-plane primitive vectors $\mathbf{t}_1$ and $\mathbf{t}_2$ and reciprocal lattice vectors $\mathbf{g}_1$ and $\mathbf{g}_2$. The *symmetry allowed* coupling of two single layer states $(i_1, \mathbf{k}_1)$ and $(i_2, \mathbf{k}_2)$, governed by $\mathbf{g}_1$ and $\mathbf{g}_2$, can, therefore, be dramatically different for very similar $\theta$. As the electronic structure of the bilayer is determined by the coupling of single layer states through the interlayer interaction, this situation is counterintuitive: one would expect electronic properties to depend smoothly on the rotation angle.

Recalling the analysis of Sec. III C, we note that the magnitude of the interlayer coupling is determined by the selection rule, Eq. (28), for the coefficients of the Fourier expansion of interlayer matrix elements, see Eq. (27). As has been discussed, the coefficients in such a Fourier expansion decay with increasing $\mathbf{G}_{1,2}$ and are largest at or near the origin of reciprocal space. Now, the shift term of, e.g., Eq. (31) describes a *scale relation* between the resulting shift of allowed $\mathbf{G}$ vectors in the Fourier sum, and the $\mathbf{k}$-vector difference of the coupled states $\mathbf{k}_2 - \mathbf{k}_1$: states coupled by $2p/\gamma(i_1\mathbf{g}_1 + i_2\mathbf{g}_2)$ correspond to a shift of $-(i_1, i_2)$. Thus it is not the $\mathbf{g}_i$ that control how single layer states couple, but rather the vectors $\mathbf{g}_i^{(c)} = 2p/\gamma\mathbf{g}_i$.

This is illustrated in Fig. 4. Shown in the central panel are the UBZ, RBZ, and BBZ of the $(p,q)=(11,31)$ twist bilayer (rotation angle $\theta = 23.16°$). Indicated are two different possible couplings of single layer states: (i) $\mathbf{k}_2 - \mathbf{k}_1 = \mathbf{g}_2$, and (ii) $\mathbf{k}_2 - \mathbf{k}_1 = 11\mathbf{g}_1 = \mathbf{g}_1^{(c)}$. The solution vectors of $\mathbf{G}_1 = R\mathbf{G}_2 + \mathbf{k}_2 - \mathbf{k}_1$ corresponding to each of these cases are shown in the left- and right-hand side panels, respectively. The single layer states coupled by $\mathbf{g}_1^{(c)}$ have contributing vectors close to the origin indicating a strong coupling, while the states coupled by $\mathbf{g}_2$ have contributing vectors far from the origin, indicating a comparatively weaker coupling.

The extent to which states connected by $\mathbf{g}_i^{(c)}$ dominate other symmetry allowed couplings depends on the nature of the decay of the Fourier coefficients $C_{\mathbf{k}_1+\mathbf{G}_1}^{\mathbf{k}_2+R\mathbf{G}_2}$, i.e., on details of the electronic structure. For graphene, as we show in Sec. IV, the situation is of a coupling dominated entirely by the

vectors $\mathbf{k}_2 - \mathbf{k}_1 = n_1\mathbf{g}_1^{(c)} + n_2\mathbf{g}_2^{(c)}$ with $0 \leq n_i \leq 1$. Regardless of the particular details of the Fourier coefficients, allowing $|\mathbf{t}_i| \to \infty$ and $|\mathbf{g}_i| \to 0$ for a given rotation angle $\theta$, beyond a certain point, introduces no new interlayer coupling to the bilayer system as all additional symmetry allowed couplings will have zero magnitude by the arguments above. Thus the ultimate smoothness of electronic properties with $\theta$ is guaranteed by the fact of the decay the Fourier coefficients $C_{\mathbf{k}_1+\mathbf{G}_1}^{\mathbf{k}_2+R\mathbf{G}_2}$, a natural result. Clearly, the faster the decay of these coefficients the greater the dominance of a few $\mathbf{g}_i^{(c)}$ in the coupling of single layer states and, hence, the less the electronic structure depends on details of the real space cell.

To determine a general form of the $\mathbf{g}_i^{(c)}$, we first calculate $g = |\mathbf{g}_i|$ which, for $\delta = 1$ is given by

$$g = \frac{2\gamma}{\sqrt{9(p^2+3q^2)}} = \frac{2\gamma}{3p}\sin\theta/2 = \frac{2\gamma}{3\sqrt{3}q}\cos\theta/2. \quad (41)$$

and for $\delta = 3$ by

$$g = \frac{2\gamma}{\sqrt{3(p^2+3q^2)}} = \frac{2\gamma}{\sqrt{3}p}\sin\theta/2 = \frac{2\gamma}{3q}\cos\theta/2. \quad (42)$$

To determine $g^{(c)} = |\mathbf{g}_i^{(c)}|$ we then multiply $g$ by the inverses of the prefactors to the shift terms in Eqs. (29)–(32), i.e., by $6q/\gamma$, $6\sqrt{3}p/\gamma$, $2p/\gamma$, and $6\sqrt{3}q/\gamma$, respectively [the factors of $\sqrt{3}$ arise from the different $(l_1 - 2l_2, 2l_1 - l_2)^T$ structure of Eqs. (30) and (32)]. In this way we find that the relevant $g^{(c)}$ is given by

$$g^{(c)} = \frac{4\sqrt{3}}{\delta}\sin\frac{\theta}{2}, \quad (43)$$

and that $\mathbf{g}_i^{(c)} = g^{(c)}\hat{\mathbf{g}}_i$ with $\hat{\mathbf{g}}_i$ the unit vectors formed from the primitive vectors $\mathbf{g}_i$. As expected, these coupling vectors depend only on the misorientation angle. Interestingly, $g^{(c)}$ may be expressed in terms of $\Delta K$, i.e., in terms of the separation of pairs of special $K$ points $(\mathbf{K}_U, \mathbf{K}_R)$, see Fig. 3, as

$$g^{(c)} = \frac{3\sqrt{3}}{\delta}\Delta K. \quad (44)$$

In Ref. 9 it was noted that $\Delta K$ constitutes an energy scale of the twist layer physics. Here, in our more general lattice treatment, we see that this is also an important reciprocal space length scale, describing the coupling of single layer states by the interaction.

### F. Reduction in Fermi velocity of the Dirac cones

Here we examine the impact upon the degenerate Dirac cones of the bilayer of the nonzero matrix elements. Let us consider the Dirac cone state from the unrotated layer situated at $\mathbf{K}_U + \delta\mathbf{k}$ which, therefore, has eigenvalue

$$\epsilon^{(1)} = s_1|\delta\mathbf{k}|, \quad (45)$$

where we set $\hbar v_F = 1$, and $s_1$ is a sign indicating whether the eigenvalue belongs to the electron or hole Dirac cone. From Sec. III C we know that this state will couple with the two states from the rotated layer Dirac cone also having $\mathbf{k}$ vector $\mathbf{K}_U + \delta\mathbf{k}$. These states have energies

$$\epsilon^{(2)} = s_2 |\delta\mathbf{k} - \Delta\mathbf{K}|. \tag{46}$$

In this equation $\Delta\mathbf{K}$ is a reciprocal space vector connecting nearest neighbor Dirac cones (for $\theta < 30°$ that we consider here), see Fig. 3. Due to the translational symmetry, there may also be coupling with states at $\mathbf{K}_U + \delta\mathbf{k} - n_1\mathbf{g}_1^{(c)} - n_2\mathbf{g}_2^{(c)}$ which have energies

$$\epsilon_{n_1 n_2}^{(2)} = s_2 |\delta\mathbf{k} - \Delta\mathbf{K} - n_1\mathbf{g}_1^{(c)} - n_2\mathbf{g}_2^{(c)}|, \tag{47}$$

where $n_{1,2}$ are integers. Note the use the coupling vectors $\mathbf{g}_i^{(c)}$, that determine which single layer states couple through the interlayer interaction, see Sec. III E. Choosing $\delta = 3$ we find from Eq. (44) that

$$\mathbf{g}_1^{(c)} = \sqrt{3}\Delta K \hat{\mathbf{g}}_1, \tag{48}$$

$$\mathbf{g}_2^{(c)} = \sqrt{3}\Delta K \hat{\mathbf{g}}_2, \tag{49}$$

with $\hat{\mathbf{g}}_1$ and $\hat{\mathbf{g}}_2$ the unit vectors of the bilayer reciprocal lattice. Using this one may then show that

$$|\Delta\mathbf{K} + n_1\mathbf{g}_1^{(c)} + n_2\mathbf{g}_2^{(c)}| = \Delta K \eta_{n_1 n_2}, \tag{50}$$

where

$$\eta_{n_1 n_2}^2 = 1 + n_1 n_2 + 3(n_1 - n_2)(n_1 - n_2 - 1), \tag{51}$$

i.e., that the $\theta$ dependence of $|\Delta\mathbf{K} + n_1\mathbf{g}_1^{(c)} + n_2\mathbf{g}_2^{(c)}|$ is *entirely through* $\Delta K$. We may then expand $\epsilon_{n_1 n_2}^{(2)}$ as

$$(\epsilon_{n_1 n_2}^{(2)})^2 = \delta k^2 + \Delta K^2 \eta_{n_1 n_2}^2 - 2\delta k \Delta K \eta_{n_1 n_2} \cos \phi_{n_1 n_2}. \tag{52}$$

In this expression $\phi = \angle(\delta\mathbf{k}, \Delta\mathbf{K} + n_2\mathbf{g}_1^{(c)} + n_2\mathbf{g}_2^{(c)})$, and $\delta k = |\delta\mathbf{k}|$. The overall eigenvalue shift may be written to second order as

$$\delta\epsilon = \sum_{n_1 n_2} \left\{ \frac{\alpha_{n_1 n_2}^{s_1 -}}{\epsilon^{(1)} + \epsilon_{n_1 n_2}^{(2)}} + \frac{\alpha_{n_1 n_2}^{s_1 +}}{\epsilon^{(1)} - \epsilon_{n_1 n_2}^{(2)}} \right\}, \tag{53}$$

where $\alpha_{n_1 n_2}^{s_1 -}$ and $\alpha_{n_1 n_2}^{s_1 +}$ are coupling constants between the different states (i.e., squares of overlap elements of the kind discussed in Secs. III C and III D). Finally, from Eqs. (50)–(53) may then be derived that this shift leads to a reduction in the Fermi velocity given by

$$v_F = v_F^{(SL)} \left(1 - \frac{\alpha}{\Delta K^2}\right), \tag{54}$$

where $v_F$ is the Fermi velocity of the misoriented layers, $v_F^{(SL)}$ the Fermi velocity of SLG, and $\alpha$ an overall coupling constant given by

$$\alpha = \sum_{n_1 n_2} \frac{\alpha_{n_1 n_2}^{s_1 -} + \alpha_{n_1 n_2}^{s_1 +}}{\eta_{n_1 n_2}^2}. \tag{55}$$

Thus $\alpha > 0$ as required for Eq. (54) to actually describe a reduction in the Fermi velocity.

The angle dependence contained in $\Delta K$ can, equivalently, be expressed via the moiré periodicity (see Sec. II) $D$ leading to the form

$$v_F = v_F^{(SL)}(1 - \beta D^2), \tag{56}$$

where $\beta$ is a related coupling constant.

Note that while Eq. (54) is of the same form as that derived by Santos *et al.* in Ref. 9, the origin is somewhat different. Rather than use a continuum approximation, as deployed in Ref. 9, we have retained the lattice physics which, in fact, only enters in the form of the "coupling" primitive vectors, Eqs. (48) and (49).

## IV. TIGHT-BINDING ANALYSIS

We now turn to tight-binding calculations of the twist bilayer structures elucidated in Sec. II. Given that the number of atoms in the real space commensuration cell diverges as the rotation angle $\theta \to 0°$ the tight-binding method offers perhaps the only way of exploring this interesting limit; *ab initio* calculations are certainly not practical. Here we shall employ the same tight-binding method deployed by Santos *et al.* in their continuum approach to the twist bilayer,[10] one of the so-called environment dependent tight-binding methods.[21]

In the original article by Tang *et al.* the environment dependent parameterization for carbon that these authors proposed was checked against a database including, amongst other three dimensional lattices, diamond and graphite, as well as a one dimensional carbon chain. Unfortunately, graphene and graphene-based structures were not part of this dataset, and it is thus important to first verify the accuracy of this method for this case. A sensitive test of accuracy is provided by the Dirac point splitting of graphene bilayer structures, which may be quite large in the case of the AB stacked bilayer (the *ab initio* value is 0.78 eV) and on the other hand rather small in the case of twist bilayers, e.g., 7 meV for both the $\theta = 30° \pm 8.21°$ twist bilayers.[12] This latter case entails a particularly sensitive test as, although both the $\theta = 38.21°$ and $\theta = 21.79°$ systems have the same Dirac point splitting, the crystal geometries are actually quite different.[12]

In Fig. 6 are shown calculations of the Dirac point splitting for the AB bilayer, as well as the two twist bilayers with $\theta = 30° \pm 8.21°$. Surprisingly, one finds that even the Dirac point splitting of the AB bilayer is not well reproduced; a much reduced interlayer separation is required to recover the *ab initio* result of 0.78 eV. In addition, the splitting of the $\theta = 30° \pm 8.21°$ twist bilayers is also underestimated and, furthermore, is quite different between the $\theta = 38.21°$ and $\theta = 21.79°$ cases.

Fortunately, this situation is significantly improved by switching off the environment dependence of the hopping integrals, in which case the method is simply the usual tight-binding scheme with distance dependent pairwise hopping matrix elements (see Ref. 21). Given this, a reasonable agreement with *ab initio* calculations may be found. For a somewhat reduced interlayer distance of 3.17 Å (5% smaller than the nominal experimental interlayer distance of 3.34 Å), we find $\approx 7$ meV for the twist bilayer splitting, which is in very good agreement with *ab initio* data, and a splitting of 0.63 eV for the AB bilayer, which is less good but still reasonable. This interlayer distance is indicated by a
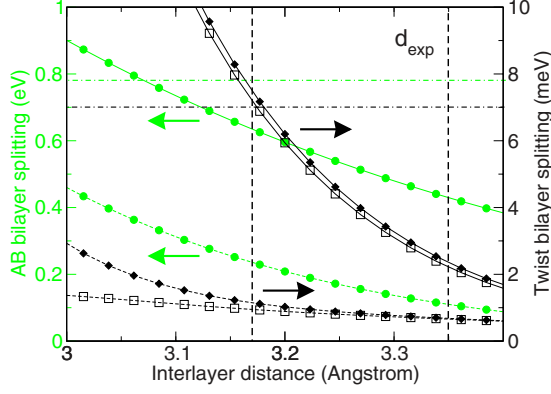
FIG. 6. (Color online) Tight-binding calculation of the Dirac point splitting in (i) AB bilayer, indicated by light shaded points and (ii) $\theta = 30° \pm 8.21$ twist bilayers, indicated by dark shaded open squares ($\theta = 38.21°$) and diamond symbols ($\theta = 21.79°$). The *ab initio* values for the AB and twist bilayer splitting are given by the horizontal dot-dashed lines. Full/dashed lines are calculations with the environment dependence of the hopping matrix elements switched off/on.

dashed vertical line in Fig. 6. Our choice of calculation method is therefore the parameterization of Tang *et al.*, but with the environment dependence suppressed, and the interlayer distance set to 3.17 Å.

While the tight-binding method extends the domain of direct band structure calculation far beyond that which may be achieved by the *ab initio* approach, for the particular case of bilayer graphene (or more generally graphene stacks) one may do significantly better. In particular, if it is only the low energy band structure that is of interest, the single layer graphene basis introduced in Sec. III is much more appropriate that the full tight-binding basis set. In this basis the bilayer Hamiltonian is

$$[\mathbf{H}(\mathbf{k})]_{i_1 \mathbf{k}_1 i_2 \mathbf{k}_2} = \begin{pmatrix} \langle \phi_{i_1 \mathbf{k}_1}^{(1)} | \mathbf{H} | \phi_{i_2 \mathbf{k}_2}^{(1)} \rangle & \langle \phi_{i_1 \mathbf{k}_1}^{(1)} | \mathbf{H} | \phi_{i_2 \mathbf{k}_2}^{(2)} \rangle \\ \langle \phi_{i_1 \mathbf{k}_1}^{(2)} | \mathbf{H} | \phi_{i_2 \mathbf{k}_2}^{(1)} \rangle & \langle \phi_{i_1 \mathbf{k}_1}^{(2)} | \mathbf{H} | \phi_{i_2 \mathbf{k}_2}^{(2)} \rangle \end{pmatrix},$$

(57)

where $i_1 \mathbf{k}_1$ and $i_2 \mathbf{k}_2$ are the band and $\mathbf{k}$ indices of states that fold back to $\mathbf{k}$ (a reciprocal lattice vector in the BBZ), and the superscript of the kets has the same meaning as in Sec. III, i.e., (1)/(2) refers to eigenkets of the unrotated/rotated layers. Eigenvalues at $\mathbf{k}$ may then be obtained by diagonalizing the matrix consisting of all states $i_1 \mathbf{k}_1$ and $i_2 \mathbf{k}_2$ that fold back to $\mathbf{k}$.

Matrix elements in Eq. (57) will involve both on-site terms and terms involving interlayer hopping integrals $\langle \phi_{i_{n'} \mathbf{k}_{n'}}^{(n')} | \overline{V} | \phi_{i_n \mathbf{k}_n}^{(n)} \rangle$ where $\overline{V} = \frac{1}{2}(V^{(1)} + V^{(2)})$. The matrix elements $\langle \phi_{i_1 \mathbf{k}_1}^{(1)} | V^{(2)} | \phi_{i_1 \mathbf{k}_1}^{(1)} \rangle$ and $\langle \phi_{i_2 \mathbf{k}_2}^{(2)} | V^{(1)} | \phi_{i_2 \mathbf{k}_2}^{(2)} \rangle$ are equivalent to three center hopping integrals, and so may be set to zero, while the matrix element $\langle \phi_{i_1 \mathbf{k}_1}^{(1)} | \overline{V} | \phi_{i_2 \mathbf{k}_2}^{(2)} \rangle$ may be evaluated as

$$\langle \phi_{i_1 \mathbf{k}_1}^{(1)} | \overline{V} | \phi_{i_2 \mathbf{k}_2}^{(2)} \rangle = \frac{1}{N_C} \sum_{n_1 n_2} e^{i \mathbf{k}_2 \cdot \mathbf{R}_{n_2}} e^{-i \mathbf{k}_1 \cdot \mathbf{R}_{n_1}} a_{i_1 \mathbf{k}_1}^{p_z} a_{i_2 \mathbf{k}_2}^{p_z} (n_z^2 t_{pp\sigma}$$

$$+ (1 - n_z^2) t_{pp\pi}).$$

(58)

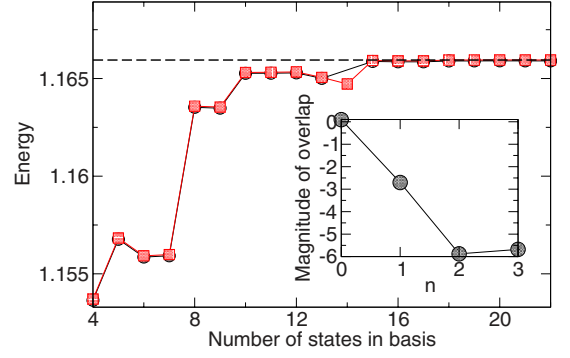where $\mathbf{R}_{n_1}$ and $\mathbf{R}_{n_2}$ are vectors from layer 1 (unrotated) and



FIG. 7. (Color online) Convergence of two nearly degenerate eigenvalues on the lower branch of the bilayer Dirac cone. The rotation angle of the bilayer is $\theta = 3.48°$ (corresponding to $(p,q) = (1, 19)$—see Sec. II). Eigenvalues are calculated at $\mathbf{k} = \mathbf{K} + \frac{2}{10}(\boldsymbol{\Gamma} - \mathbf{K})$ with $\mathbf{K}$ and $\boldsymbol{\Gamma}$ the $\mathbf{k}$ vectors of the $K$ and $\Gamma$ points. Inset shows $\log_{10} |\langle \phi_{i_1 \mathbf{k}_1}^{(1)} | \overline{V} | \phi_{i_2 \mathbf{k}_2}^{(2)} \rangle|$ plotted for $\mathbf{k}_2 - \mathbf{k}_\Gamma = n\mathbf{g}_1$.

layer 2 (rotated), respectively, the sum is over all atoms in the twist boundary primitive cell, $a_{i_n \mathbf{k}_n}^{p_z}$ is the $p_z$ coefficient of the eigenvector corresponding to the $i_n \mathbf{k}_n$ state from layer $n$, $n_z$ a directional cosine, $t_{pp\sigma}$ and $t_{pp\pi}$ distant dependent hopping integrals, and $N_C$ the number of carbon atoms in the bilayer primitive cell.

The advantage of this approach is that if it is only the low energy band structure that is of interest, then only low energy eigenkets of the unrotated and rotated layers are needed in constructing the SLG basis. In practice, the number of such low energy states required will depend on the strength of the interlayer interaction, which for graphene layers is weak and leads to a rather rapid convergence of the basis set, as shown in Fig. 7. For the case of the $\theta = 3.48°$ bilayer shown the maximum size of the basis set is 2048 states, and numerical convergence is reached at 24 states. A further advantage for the special case of twist bilayers lies in fact that from the selection rule analyzed in Sec. III C one knows that *a priori* many of the matrix elements in Eq. (57) will be zero. Inspection of the numerical value of the interlayer matrix elements, Eq. (58), shows that they are negligible for $\mathbf{k}_2 - \mathbf{k}_1 = n_1 \mathbf{g}_1^{(c)} + n_2 \mathbf{g}_2^{(c)}$ with $n_i > 1$ (see Sec. III E for a description of $\mathbf{g}_{1,2}^{(c)}$); a typical case is illustrated in the inset of Fig. 7.

For actual calculations one may then utilize a truncated basis in which only a fraction of the actual matrix elements required need be calculated. This extends by more than an order of magnitude the number of carbon atoms that may be considered: within the SLG approach $N_C = 26\,068$ could be treated within the same time that, by direct tight-binding calculations, a system of $N_C \approx 1200$ could be calculated.

We now consider the low energy electronic structure of a selection of twist bilayers, shown in Fig. 8, with the band structure plotted along the MK$\Gamma$ high symmetry points path in the BBZ. In panels 1–4 are shown four twist bilayers in the set $p = 1$, $q \in$ odd $\mathbb{Z}$ with $q = 3, 7, 25, 45$ (misorientation angles of $\theta = 21.79°$, $9.43°$, $2.65°$, and $1.47°$, respectively). In panels 1–3 are shown band structures generated by both direct tight-binding calculation as well as the SLG basis outlined above; clearly these two approaches lead to identical results, as expected. A number of interesting features may be
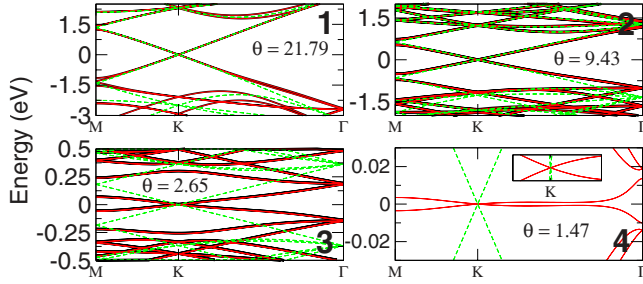
FIG. 8. (Color online) Tight-binding band structures for rotation angles of $\theta=21.79°(1,3)$, $9.43°(1,7)$, $2.65°(1,25)$, $1.47°(1,45)$, displayed, respectively, clockwise from top left. Shown is the band structure generated by direct tight-binding calculation (wide black lines) and that generated with SLG basis approach, indicated by light shaded (green) lines. For comparison in each panel the folded back band structure of single layer graphene is shown (dashed lines). The numbering of the panels corresponds to that of Fig. 3.

noted from these band structures. Firstly, as expected from the general analysis of Sec. III the Dirac point always decouples, i.e., there is no splitting of the degenerate Dirac bands from each layer, see Fig. 9. On the other hand, in agreement with *ab initio* calculations,[6,8,11] one observes that *away* from the Dirac point the bilayer band structure clearly shows a perturbation due to layer interaction, as may be observed in Fig. 8 by the strong band hybridization at the $\Gamma$ point. This, as discussed in Sec. III C, is due to the term $\mathbf{k}_2 - \mathbf{k}_1$ in the selection rule $\mathbf{G}_1 = \mathbf{R}\mathbf{G}_2 + \mathbf{k}_2 - \mathbf{k}_1$; when $\mathbf{k}_2 - \mathbf{k}_1 = 0$ the interlayer matrix elements never vanish leading to a strong coupling for these states. In addition, one notes a reduction in Fermi velocity of the Dirac cone as the rotation angle $\theta \rightarrow 0°$.

In Fig. 10 is shown this Fermi velocity suppression as a function of the rotation angle of the twist bilayer. Clearly, this effect is quite substantial, and for $\theta=1.47°$ (the smallest angle calculated) $v_F$ is only 5% of the value of SLG. Interestingly, for $\theta > 5°$ the tight-binding data are very well described by Eq. (54), in the small angle limit, however, the failure of any fitting of the form Eq. (54) indicates the im-
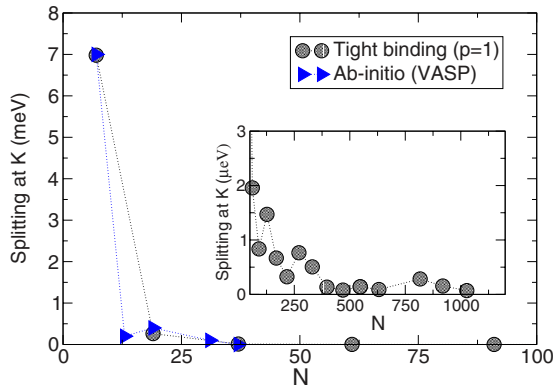


FIG. 9. (Color online) Splitting of bands at the Dirac point in misoriented graphene layers. Shown are tight-binding binding calculations for supercells generated with $p=1$ and $q$ an odd integer. First principles calculations for supercells generated by $(p,q)$ pairs of $(1,3)$, $(1,2)$, $(1,5)$, $(2,3)$, $(1,7)$ in order of increasing $N$ are taken from Ref. 11.
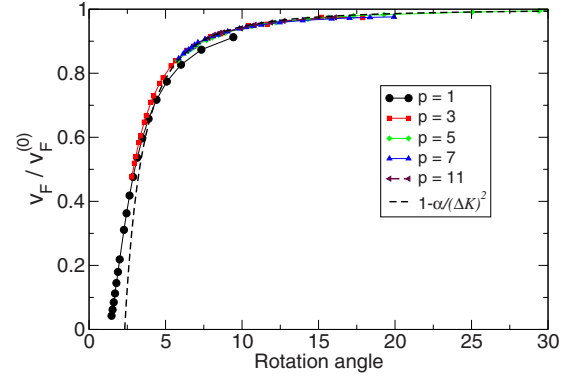


FIG. 10. (Color online) Relation between misorientation angle of the bilayer and Fermi velocity damping; dashed (black) line in the main panel is the best fit to Eq. (54) for data points with $\theta > 5°$.

portance of higher orders of perturbation theory. Clearly, the band structure in the $\theta \rightarrow 0°$ limit is profoundly altered from that of SLG with, however, the degeneracy of the Dirac bands from each layer preserved, as was proved must be the case in Sec. III D. (One should note that, in contrast to the first principles calculation of Ref. 12, we find a small reduction in Fermi velocity for the case of $\theta=9.43°$; such a difference presumably reflects the fact that parameterization of Tang *et al.*,[21] not explicitly designed for low energy graphene physics, has scope for improvement.)

As has been mentioned, this preservation of the degeneracy is a striking illustration of the singular nature of the $\theta \rightarrow 0°$ limit; for any finite $\theta$ one has a *fourfold* degeneracy at the Dirac point, while at $\theta=0$ one has the AB bilayer with a twofold degeneracy at the Dirac point, and with the other Dirac bands split by 0.78 eV. An interesting question, which we shall only pose here and not answer, is how this Fermi velocity reduction would be altered by both charge self-consistency and many-body effects. Both of these may be expected to become more important as the Fermi velocity is reduced, and may dramatically change the nature of the small angle electronic structure.

Graphene stacks grown on the C face of SiC typically have Fermi velocity reductions of 20–30 % which then implies, assuming that such a reduction is entirely due to rotation, misorientations of $\theta > 5°$. Given that the formation energy of a twist bilayer increases as $\theta \rightarrow 0°$,[13] with the minimum defect energy for $30° \pm 2.20°$,[12] it makes sense that, on average, misorientation angles with $\theta < 5°$ should play a less important role. On the other hand, it is clear that samples with $\theta < 5°$ do exist; scanning tunnel microscopy experiments detect moiré patterns that correspond to angles in the $1.9°-19°$ range.[7] In contrast, for a graphene slab dominated by $30° \pm 2.02°$ rotations, or simply large angle rotations (such a system was studied in Ref. 6, see also Ref. 22) one would expect to have, in addition to a Dirac spectrum over a wide energy range, a Fermi velocity exactly that of SLG.

## V. CONCLUSIONS

To conclude we have given a complete description of the possible commensurations of graphene layers misoriented by

some angle $\theta$. We find that the condition for a commensuration to occur is that, expressed in lattice coordinates of the unrotated layer, the rotation matrix connecting the layers be rational valued, and thus the complete set of commensurations is described by two integers, which we denote $(p,q)$. For any such bilayer, we have shown that the $K$ points of the unrotated and rotated layers map directly to $K$ points of the bilayer Brillouin zone; a fact that plays an important role in the interlayer interaction.

We have further shown that the nature of the interlayer interaction may be understood by a **k**-dependent interference condition that may be expressed as a commensuration of the single layer reciprocal lattices. This guarantees the decoupling of the Dirac point and the degeneracy in the Dirac cones from each layer, but does not preclude interactions between all states. These latter interactions in fact give rise to a reduction of the Fermi velocity in the $\theta \to 0°$ limit, and we find a form of this Fermi damping which agrees with that presented by Santos *et al.*,[10] although our derivation is independent of any continuum approximation. As an interesting consequence of this analysis, we are able to show that the bilayer electronic structure will, in general, depend only on the misorientation angle of the layers and not on the details of the real space unit cell.

To complement this general analysis we have calculated band structures of a wide range of graphene twist bilayers via the tight-binding method. By the introduction of a basis of single layer graphene eigenkets, which we show to be significantly more efficient for the case of the twist bilayer, we are able to probe the band structure in the small angle limit with relative computational ease. We find Fermi velocity reduction that, for rotation angles in the range $5° < \theta < 30°$ agrees very well with the form presented here and in Ref. 9, but that for $\theta < 5°$, where at $\theta = 1.47°$ the Fermi velocity is only 5% of the SLG value, the reduction cannot be described in this way. In fact, the Dirac bands in the small angle limit, while guaranteed to be degenerate, show nonlinear distortion away from the Dirac point. Thus the graphene twist bilayer encompasses a wide range of electronic behavior, from essentially SLG behavior for large angle rotations to quite different behavior in the small angle limit which, nevertheless, shares important features with the large angle case. While small angle rotations[7] (as low as 1.9°) have been observed experimentally, the electronic properties of such low angle misoriented layers has yet to be experimentally explored. The possibility of a graphene type behavior different from both SLG and the AB bilayer makes interesting the further study of this low angle limit.

### APPENDIX A: DERIVATION OF THE COMMENSURATION LATTICE PRIMITIVE VECTORS

In this appendix we wish to determine the primitive lattice vectors of the commensuration lattice given by Eq. (11), i.e., the lattice defined by

$$\mathbf{m} = \alpha \begin{pmatrix} -p + 3q \\ 2p \end{pmatrix} + \beta \begin{pmatrix} -2p \\ p + 3q \end{pmatrix}. \tag{A1}$$

We first notice that only coprime $p,q$ correspond to unique solutions. Given this, a necessary condition for recovering lattice vectors is obviously the elimination of the greatest common divisor (gcd) of the components of all the (integer valued) vectors in Eqs. (11) and (12). This leads to following commensuration primitive vectors:

$$\mathbf{t}_1 = \frac{1}{\gamma} \begin{pmatrix} p + 3q \\ -2p \end{pmatrix}, \quad \mathbf{t}_2 = \frac{1}{\gamma} \begin{pmatrix} 2p \\ -p + 3q \end{pmatrix} \tag{A2}$$

with $\gamma = \gcd(3q + p, 3q - p)$, and where we have used the fact that $\gcd(x, y) = \gcd(x + cy, y)$ with $c$ an arbitrary integer. Possible values of $\gamma$ involve the additional parameter $\delta = 3/\gcd(p, 3)$, and are displayed in Table I.

To prove that these are indeed the primitive vectors requires further that there is no linear combination of them yields *integer valued vectors* of smaller length. In fact, as we will now show, the vectors given in Eq. (A2) are primitive only for the case where $\delta = 1$, and that when $\delta = 3$ it is the linear combinations $1/3(-\mathbf{t}_1 + 2\mathbf{t}_2)$ and $1/3(-2\mathbf{t}_1 + \mathbf{t}_2)$ that form the primitive vectors of the commensuration lattice.

We first take a linear combination of the supposed primitive vectors as follows:

$$\frac{\alpha_i}{N_i} \mathbf{t}_1 + \frac{\beta_i}{N_i} \mathbf{t}_2 = \mathbf{t}_i', \tag{A3}$$

where $\alpha_i, \beta_i, N_i \in \mathbb{Z}$ and the index $i = 1, 2$. By eliminating common factors of $\alpha_i$ and $\beta_i$ from $N_i$ we may choose $\gcd(\alpha_i, \beta_i) = 1$. Defining $t = |\mathbf{t}_1| = |\mathbf{t}_2|$ and $t' = |\mathbf{t}_1'| = |\mathbf{t}_2'|$, $\mathbf{t}_1$ and $\mathbf{t}_2$ are primitive only if there exists no $\alpha_i, \beta_i, N_i$ such that $t' < t$. Suppose that for a given set of these parameters $t' > t$ then we may write

$$N_i t < N_i t' = |\alpha_i \mathbf{t}_1 + \beta_i \mathbf{t}_2| \leq (|\alpha_i| + |\beta_i|)t \tag{A4}$$

so that if $t' > t$ then $|\alpha_i| + |\beta_i| > N_i$ and hence $|\alpha_i| + |\beta_i| < N_i$ implies $t' < t$. Thus if there exist $\alpha_i, \beta_i, N_i$ such that $|\alpha_i| + |\beta_i| < N_i$ *and* the linear combinations Eq. (A3) remain integer valued then the supposed primitive vectors $\mathbf{t}_1$ and $\mathbf{t}_2$ are in fact not primitive.

From Eq. (A2) and Eq. (A3) we find

$$\left[ \frac{(\alpha_i + 2\beta_i)}{\gamma N_i} p + \frac{3\alpha_i}{\gamma N_i} q \right] = z_1, \tag{A5}$$

$$-\left[ \frac{(2\alpha_i + \beta_i)}{\gamma N_i} p - \frac{3\beta_i}{\gamma N_i} q \right] = z_2, \tag{A6}$$

where $z_1, z_2 \in \mathbb{Z}$ in order that $\mathbf{t}_i'$ be integer valued. As $\gcd(\alpha_i, \beta_i) = 1$ and $\gcd(p, q) = 1$, then for $z_{1,2}$ to be integer valued as claimed we require $\gamma N_i$ to be a common factor of the coefficients of $p$ and $q$ on the left-hand sides of Eqs. (A5) and (A6). Using the fact that $\gcd(\alpha_i, \beta_i) = 1$, we find that possible values of $\gcd(3\alpha_i, \alpha_i + 2\beta_i)$ and $\gcd(3\beta_i, 2\alpha_i + \beta_i)$ are 1, 2, 3, and 6. Therefore, as the minimum possible value of $\gamma = 1$, then the maximum possible value of $N_i$ is 6. As $|\alpha_i| + |\beta_i| < N_i$ this in turn restricts the possible values of $\alpha_i, \beta_i$.

We have used the requirement that $\mathbf{t}_i'$ be integer valued to place a condition $\gamma N_i \leq 6$, not $N_i \leq 6$, and hence we need to eliminate $(\alpha_i, \beta_i, N_i)$ that lead to noninteger $\mathbf{t}_i'$. From the full set of $\{(\alpha_i, \beta_i, N_i)\}$ this then leaves only the cases $(\alpha_i, \beta_i, N_i) = \{(1,1,3), (-1,2,3), (-2,1,3)\}$, and using these latter two we finally find the new primitive vectors

$$\mathbf{t}_1 = \frac{1}{\gamma}\begin{pmatrix} -p-q \\ 2q \end{pmatrix}, \quad \mathbf{t}_2 = \frac{1}{\gamma}\begin{pmatrix} 2q \\ -q+q \end{pmatrix}, \qquad \text{(A7)}$$

However, for the case $\delta = 1$ then we have $3 | \gamma$ and $3 | p$ and since $\gcd(p,q) = 1$ then $3 \nmid q$ and $\mathbf{t}_1$ and $\mathbf{t}_2$ given by Eq. (A7) cannot be integer valued. Hence for $\delta = 1$ then Eq. (A2) are already the primitive vectors of the commensuration lattice. On the other hand if $\delta = 3$ then if both $p$ and $q$ are odd then $\gamma = 2$ and $\mathbf{t}_1$ and $\mathbf{t}_2$ given by Eq. (A7) are integer valued while if one of $p, q$ is even then $\gamma = 1$ and again this is so.

To summarize we find that for the case $\delta = 1$ the vectors given by Eq. (A2) are already primitive, while for the case $\delta = 3$ instead Eq. (A7) gives the primitive vectors.

## APPENDIX B: SOLUTION OF EQUATION $\mathbf{G}_1 = \mathbf{R}\mathbf{G}_2 + (\mathbf{k}_2 - \mathbf{k}_1)$

We wish to determine the solutions to the equation

$$\mathbf{G}_1 = \mathbf{R}\mathbf{G}_2 + (\mathbf{k}_2 - \mathbf{k}_1). \qquad \text{(B1)}$$

This represents a similar equation to the real space commensuration equation, but with an additional term $(\mathbf{k}_2 - \mathbf{k}_1)$. Utilizing the coordinate system of the unrotated reciprocal lattice we may write $\mathbf{G}_1 = m_1 \mathbf{b}_1 + m_2 \mathbf{b}_2$ and $\mathbf{G}_2 = n_1 \mathbf{b}_1 + n_2 \mathbf{b}_2$ where $\mathbf{m} = (m_1, m_2)^T$ and $\mathbf{n} = (n_1, n_2)^T$ must be integer valued. Furthermore, the term $(\mathbf{k}_2 - \mathbf{k}_1)$ is integer valued in the coordinate system of the bilayer reciprocal lattice, i.e., $(\mathbf{k}_2 - \mathbf{k}_1) = l_1 \mathbf{g}_1 + l_2 \mathbf{g}_2$. The transformation from the bilayer to unrotated reciprocal lattice coordinate systems is

$$\mathbf{T}_{BU} = \frac{\gamma}{i_3}\begin{pmatrix} -p+q & -2q \\ 2q & -p-q \end{pmatrix} \qquad \text{(B2)}$$

and the rotation operator, transformed to the unrotated reciprocal lattice coordinate system, is be found to be

$$\mathbf{R}_L = \frac{1}{i_3}\begin{pmatrix} i_2 + i_1 & -2i_1 \\ 2i_1 & i_2 - i_1 \end{pmatrix}, \qquad \text{(B3)}$$

where, as before, we have

$$i_1 = 2pq, \qquad \text{(B4)}$$

$$i_2 = 3q^2 - p^2, \qquad \text{(B5)}$$

$$i_3 = 3q^2 + p^2. \qquad \text{(B6)}$$

Using these we may rewrite Eq. (B1) as

$$\begin{pmatrix} m_1 \\ m_2 \end{pmatrix} = \frac{1}{i_3}\begin{pmatrix} i_2 + i_1 & -2i_1 \\ 2i_1 & i_2 - i_1 \end{pmatrix}\begin{pmatrix} n_1 \\ n_2 \end{pmatrix}$$
$$+ \frac{\gamma}{i_3}\begin{pmatrix} -p+q & -2q \\ 2q & -p-q \end{pmatrix}\begin{pmatrix} l_1 \\ l_2 \end{pmatrix}. \qquad \text{(B7)}$$

Our solution of this equation is based on diagonalizing $\mathbf{R}_L$

and $\mathbf{T}_{BU}$ which, it turns out, may be simultaneously diagonalised. We find the eigenvalues of $\mathbf{R}_L$ to be

$$a_\pm = -\frac{p \pm i\sqrt{3}q}{p \mp i\sqrt{3}q} \qquad \text{(B8)}$$

and those of $\mathbf{T}_{BU}$ to be

$$b_\pm = \frac{-\gamma}{p \mp i\sqrt{3}q}. \qquad \text{(B9)}$$

The eigenvectors in *both cases* are given by

$$u_\pm = \frac{1}{\sqrt{2}}\begin{pmatrix} \frac{1}{2}(1 \mp i\sqrt{3}) \\ 1 \end{pmatrix}. \qquad \text{(B10)}$$

Using these results we may rewrite Eq. (B7) as

$$\mathbf{U}^{-1}\mathbf{m} = (\mathbf{U}^{-1}\mathbf{R}_L\mathbf{U})\mathbf{U}^{-1}\mathbf{n} + (\mathbf{U}^{-1}\mathbf{T}_{CU}\mathbf{U})\mathbf{U}^{-1}\mathbf{l}. \qquad \text{(B11)}$$

Equating the real and imaginary parts of this equation we find

$$(n_2 + m_2)p = [(2n_1 - n_2) - (2m_1 - m_2)]q - \gamma l_2, \qquad \text{(B12)}$$

$$[(2n_1 - n_2) + (2m_1 - m_2)]p = (m_2 - n_2)3q - \gamma(2l_1 - l_2), \qquad \text{(B13)}$$

and by introducing the new variables $n_3 = 2n_1 - n_2$ and $m_3 = 2m_1 - m_2$ we can recast these equations as a Diophantine problem,

$$(m_2 + n_2)p = (n_3 - m_3)q - \gamma l_2, \qquad \text{(B14)}$$

$$(n_3 + m_3)p = (m_2 - n_2)3q - \gamma(2l_1 - l_2). \qquad \text{(B15)}$$

By absorbing the terms involving $\gamma$ either in the coefficient of $p$ or $q$ these equations may now be solved by inspection giving

$$\left(m_2 + n_2 + \frac{\gamma l_2}{p}\right)p = (n_3 - m_3)q, \qquad \text{(B16)}$$

$$\left(n_3 + m_3 + \frac{\gamma(2l_1 - l_2)}{p}\right)p = (m_2 - n_2)3q, \qquad \text{(B17)}$$

which leads to the solutions

$$\mathbf{n} = \alpha\frac{1}{\gamma}\begin{pmatrix} p+q \\ 2p \end{pmatrix} + \beta\frac{1}{\gamma}\begin{pmatrix} 2q \\ -p+q \end{pmatrix} - \frac{\gamma}{2p}\begin{pmatrix} l_1 \\ l_2 \end{pmatrix} \qquad \text{(B18)}$$

and

$$\mathbf{m} = \alpha\frac{1}{\gamma}\begin{pmatrix} -p+q \\ 2q \end{pmatrix} + \beta\frac{1}{\gamma}\begin{pmatrix} 2q \\ p+q \end{pmatrix} - \frac{\gamma}{2p}\begin{pmatrix} l_1 \\ l_2 \end{pmatrix} \qquad \text{(B19)}$$

with $\alpha$ and $\beta$ integers. Note that we have immediately written down the solution in terms of primitive vectors; which may be done in a similar fashion to the real space case (Appendix A).

Alternatively we may write

$$(m_2 + n_2)p = \left(n_3 - m_3 - \frac{\gamma l_2}{q}\right)q, \qquad \text{(B20)}$$

$$(n_3 + m_3)p = \left( m_2 - n_2 - \frac{\gamma(2l_1 - l_2)}{q} \right) 3q, \quad \text{(B21)}$$

which in turn leads to the solutions

$$\mathbf{n} = \alpha \frac{1}{\gamma} \begin{pmatrix} p+q \\ 2q \end{pmatrix} + \beta \frac{1}{\gamma} \begin{pmatrix} 2q \\ -p+q \end{pmatrix} - \frac{\gamma}{6q} \begin{pmatrix} l_1 - 2l_2 \\ 2l_1 - l_2 \end{pmatrix}$$
$$\text{(B22)}$$

and

$$\mathbf{m} = \alpha \frac{1}{\gamma} \begin{pmatrix} -p+q \\ 2q \end{pmatrix} + \beta \frac{1}{\gamma} \begin{pmatrix} 2q \\ p+q \end{pmatrix} + \frac{\gamma}{6p} \begin{pmatrix} l_1 - 2l_2 \\ 2l_1 - l_2 \end{pmatrix}.$$
$$\text{(B23)}$$

The case where $\delta = 1$ proceeds in exactly the same manner, the only difference being a different form for the transformation matrix $\mathbf{T}_{BU}$. The solutions are then found to be

$$\mathbf{n} = \alpha \frac{1}{\gamma} \begin{pmatrix} -p+3q \\ -2p \end{pmatrix} + \beta \frac{1}{\gamma} \begin{pmatrix} 2p \\ p+3q \end{pmatrix} - \frac{\gamma}{6q} \begin{pmatrix} l_1 \\ l_2 \end{pmatrix}, \quad \text{(B24)}$$

$$\mathbf{m} = \alpha \frac{1}{\gamma} \begin{pmatrix} p+3q \\ 2p \end{pmatrix} + \beta \frac{1}{\gamma} \begin{pmatrix} -2p \\ -p+3q \end{pmatrix} + \frac{\gamma}{6q} \begin{pmatrix} l_1 \\ l_2 \end{pmatrix} \quad \text{(B25)}$$

and

$$\mathbf{n} = \alpha \frac{1}{\gamma} \begin{pmatrix} -p+3q \\ -2p \end{pmatrix} + \beta \frac{1}{\gamma} \begin{pmatrix} 2p \\ p+3q \end{pmatrix} + \frac{\gamma}{6p} \begin{pmatrix} l_1 - 2l_2 \\ 2l_1 - l_2 \end{pmatrix},$$
$$\text{(B26)}$$

$$\mathbf{m} = \alpha \frac{1}{\gamma} \begin{pmatrix} p+3q \\ 2p \end{pmatrix} + \beta \frac{1}{\gamma} \begin{pmatrix} -2p \\ -p+3q \end{pmatrix} + \frac{\gamma}{6p} \begin{pmatrix} l_1 - 2l_2 \\ 2l_1 - l_2 \end{pmatrix}.$$
$$\text{(B27)}$$

*phsss@tfkp.physik.uni-erlangen.de

[1] A. K. Geim and K. S. Novoselov, Nature Mater. **6**, 183 (2007).

[2] C. Berger, Z. Song, X. Li, X. Wu, N. Brown, C. Naud, D. Mayou, T. Li, J. Hass, A. N. Marchenkov, E. H. Conrad, P. N. First, and W. A. de Heer, Science **312**, 1191 (2006).

[3] T. Ohta, A. Bostwick, T. Seyller, K. Horn, and E. Rotenberg, Science **313**, 951 (2006).

[4] W. A. de Heer, C. Berger, X. Wu, P. N. First, E. H. Conrad, X. Li, T. Li, M. Sprinkle, J. Hass, M. L. Sadowski, M. Potemski, and G. Martinez, Solid State Commun. **143**, 92 (2007).

[5] K. V. Emtsev, F. Speck, Th. Seyller, L. Ley, and J. D. Riley, Phys. Rev. B **77**, 155303 (2008).

[6] J. Hass, F. Varchon, J. E. Millán-Otoya, M. Sprinkle, N. Sharma, W. A. de Heer, C. Berger, P. N. First, L. Magaud, and E. H. Conrad, Phys. Rev. Lett. **100**, 125504 (2008).

[7] F. Varchon, P. Mallet, L. Magaud, and J.-Y. Veuillen, Phys. Rev. B **77**, 165415 (2008).

[8] Sylvain Latil, Vincent Meunier, and Luc Henrard, Phys. Rev. B **76**, 201402(R) (2007).

[9] W. Kohn, Phys. Rev. Lett. **76**, 3168 (1996).

[10] Z. Ni, Y. Wang, T. Yu, Y. You, and Z. Shen, Phys. Rev. B **77**, 235403 (2008).

[11] P. Poncharal, A. Ayari, T. Michel, and J.-L. Sauvajol, Phys. Rev. B **78**, 113407 (2008).

[12] S. Shallcross, S. Sharma, and O. A. Pankratov, Phys. Rev. Lett. **101**, 056803 (2008).

[13] S. Shallcross, S. Sharma, and O. A. Pankratov, J. Phys.: Condens. Matter **20**, 454224 (2008).

[14] E. Cisternas, M. Flores, and P. Vargas, Phys. Rev. B **78**, 125406 (2008).

[15] G. de Laissardiére, D. Mayou, and L. Magaud, arXiv:0904.1233 (unpublished).

[16] J. M. Campanera, G. Savini, I. Suarez-Martinez, and M. I. Heggie, Phys. Rev. B **75**, 235449 (2007).

[17] M. A. Fortes, Acta Crystallogr., Sect. A: Found. Crystallogr. **39**, 351 (1983).

[18] J. Steuding, *Diophantine Analysis* (Chapman and Hall/CRC, London, 2005).

[19] H. Beyer, M. Muller, and Th. Schimmel, Appl. Phys. A: Mater. Sci. Process. **68**, 163 (1999).

[20] C.-H. Park, L. Wang, Y.-W. Son, M. L. Cohen, and S. G. Louie, Nature Physics **4**, 213 (2008).

[21] M. S. Tang, C. Z. Wang, C. T. Chan, and K. M. Ho, Phys. Rev. B **53**, 979 (1996).

[22] M. Sprinkle, D. Siegel, Y. Hu, J. Hicks, P. Soukiassian, A. Tejeda, A. Taleb-Ibrahimi, P. Le Fevre, F. Bertran, C. Berger, W. de Heer, A. Lanzara, and E. Conrad, Phys. Rev. Lett. **103**, 226803 (2009).